ADVANCED MATERIALS TECHNOLOGIES
www.advmattechnol.de

Review and Prospects of PEM Water Electrolysis at Elevated Temperature Operation

*Marco Bonanno, Karsten Müller, Boris Bensmann, Richard Hanke-Rauschenbach, David Aili, Tanja Franken, Andreas Chromik, Retha Peach, Anna T. S. Freiberg, and Simon Thiele**

Polymer electrolyte membrane water electrolyzers (PEMWE) are currently restricted to an operating temperature range between 50 to 80 °C. This review shows that elevated temperature (ET) above 90 °C can be advantageous with respect to i) reduced cell voltages, ii) a reduction of catalyst loading or possibly the employment of less noble electrocatalysts, and iii) a greater potential for waste heat utilization when the electrolyzer is operated in exothermal mode (when the cell voltage is higher than the thermoneutral voltage). Together with presenting an overview of the materials and components utilized in elevated temperature PEMWE under liquid and steam operation, this article summarizes the experimental and modeling performances reported to date, highlights the challenges ahead, and suggests aspects, which will need to be considered to improve the performance at elevated temperature. Key points, which arise from this work are the extensive need of re-assessing the material selection both for the cell components and also at a system level, the effects and optimization of working with steam operation, and in the long run, the need for techno-economic analyses to ultimately assess whether efficiency gains will truly translate to a cost-effective technology alternative.

1. Introduction

The production of hydrogen from non-polluting renewable energy is expected to play an important role in limiting the use of fossil fuels in energy applications.[1–3] Hydrogen can be produced via water electrolysis in multiple ways,[4] namely: 1) Alkaline Water Electrolyzers (AWE), 2) Anion Exchange Membrane Water Electrolyzers (AEMWE), 3) Proton Exchange Membrane Water Electrolyzers (PEMWE), 4) Solid Oxide Electrolysis Cell (SOEC), and 5) Proton Conducting Ceramic Electrolyzers (PCCEL).

In AWE, a cell consists of two metallic electrodes immersed in an aqueous liquid electrolyte, and a porous diaphragm, which conducts hydroxyl ions is used as separator.[4] AWE are particularly advantageous in that hydrogen production does not depend on the use of Platinum Group Metals (PGM) as catalysts in the electrodes. While the relative simplicity and low system cost of AWE[5] have allowed its industrial deployment worldwide, AWE suffers from poor handling of load fluctuations, which are customary when coupling to renewable energy sources. These are hence mainly operated in the low current density region up to 500 mA cm^{-2}.[4,5] A constant struggle in AWE is to minimize the distance between the

M. Bonanno, R. Peach, A. T. S. Freiberg, S. Thiele
Helmholtz-Institute Erlangen-Nuremberg for Renewable Energy (IEK-11)
Forschungszentrum Jülich GmbH
Cauerstraße 1, 91058 Erlangen, Germany
E-mail: si.thiele@fz-juelich.de

M. Bonanno, A. T. S. Freiberg, S. Thiele
Department of Chemical and Biological Engineering
Friedrich-Alexander University Erlangen-Nuremberg
Egerlandstraße 3, 91058 Erlangen, Germany

K. Müller
Institute of Technical Thermodynamics
University of Rostock
Albert-Einstein-Straße 2, 18059 Rostock, Germany

The ORCID identification number(s) for the author(s) of this article can be found under https://doi.org/10.1002/admt.202300281

DOI: 10.1002/admt.202300281

B. Bensmann, R. Hanke-Rauschenbach
Institute of Electric Power Systems
Leibniz University Hannover
Appelstraße 9a, 30167 Hannover, Germany

D. Aili
Department of Energy Conversion and Storage
Technical University of Denmark (DTU)
Anker Engelunds Vej 301, Kongens Lyngby 2800, Denmark

T. Franken
Department of Chemical and Biological Engineering, Assistant Professorship Catalytic and Electrocatalytic Systems and Processes, Chair of Chemical Engineering
Friedrich-Alexander University Erlangen-Nuremberg
Egerlandstraße 3, 91058 Erlangen, Germany

A. Chromik
Riva Power Systems GmbH & Co. KG
Manfred-von-Ardenne-Allee 33, 71522 Backnang, Germany

electrodes and separator to reduce the ohmic resistance[6] while preventing mixing of product gases.

In this regard, recent efforts have led to the replacement of the conventional diaphragm with an AEM consisting of a thin, dense, non-porous polymer membrane across which hydroxide ions are transferred.[7] AEM technology still resorts to low-cost non-noble electrodes but requires lower concentrations of corrosive electrolyte circulating in the system. Moreover, the use of the membrane also allows higher purity of the product gas streams[8,9] and the possibility to store hydrogen under higher pressures.[10] On the other hand, long-term stability and operation at high current density still need to be resolved to achieve large-scale application with AEMWE.[8]

PEMWE are a membrane-based technology too, where the anode and cathode form a sandwich against a proton-conducting polymer electrolyte. The highly acidic nature of the polymer membrane calls for noble metal catalysts resistant to these harsh conditions,[4] with iridium and platinum-based catalysts used for the anode and cathode electrodes, respectively. In this process, only deionized water is circulated within the cell.[11] PEMWE are typically operated between 50 and 80 °C.[12] Albeit higher investment costs are required, PEMWE offers the acceptance of transient power loads and the capability to operate at high current densities in the multi-Ampere per square centimeter range.[13]

Operating between 700 and 900 °C, SOEC exhibits a significant potential for a reduced electrical energy demand compared to the water electrolysis technologies outlined above that are typically operated at temperature of 50–80 °C.[12,14] The electrolyte used in SOECs is generally zirconia, which has been stabilized with yttrium and scandium oxides.[4] The high temperatures involved in SOEC allow the resulting electrochemical processes to be highly efficient and reversible but thermo-mechanical stability remains a major issue which has so far restricted large-scale commercialization.[15]

PCCEL are also operated at high temperatures in the range of 300–600 °C.[4] Similar to SOEC, a Ni-in-oxide-electrolyte composite (cermet) is employed, but while SOEC is driven by the migration of oxygen ions to the anode, PCCEL utilize H^+ as the conducted ion in the electrolyte materials. Once again, PCCEL is currently still restricted to research and development due to durability issues.[16]

Each technology has its positive and negative aspects. SOEC and PCCEL are restricted to sites where heat energy at the corresponding operation temperatures is available. If available, the higher temperatures in SOEC and PCCEL offer the lowest electrical energy demand but the technology is not as mature as for PEMWE or AWE. Comparing the last two, PEMWE is typically favored over AWE due to the safer operation with liquid water, rapid system response, improved gas purity and higher performance. AEMWE is indeed a promising technology, but is too at its infancy stage. Within this context, exploring the prospects of PEMWE operated at ET operation allows to borrow favorable aspects from each technology, that is, i) benefiting from the reduced electrical energy demand accompanied with higher temperatures, ii) build on the favorable performance achieved with PEMWE, iii) gain from the technological maturity not present with AEMWE or SOEC, and iv) explore whether an elevated operating temperature window would serve as a possibility to reduce the use of PGM catalysts (compared to PEMWE as typically operated at or below 80 °C).

In the following, low temperature (LT) will hence stand for a system where the operating temperature is less than or equal to 90 °C while elevated temperature (ET) is considered for PEM-based systems studied in the temperature range between 90 and 170 °C, as shown in **Figure 1**.

2. Motivation for Opting for ET PEMWE

In the light that performance, durability, and cost are generally the three main factors considered for widespread implementation of water electrolysis for hydrogen production,[17] this section is intended to shed light on the key advantages that could possibly be enabled by operating at higher temperatures–in particular, a reduction of the specific energy demand of the electrolyzer, a reduction of catalyst loading or the employment of less noble electrocatalysts and better waste utilization when the electrolyzer is operated in exothermal mode (i.e. the cell operation voltage is above the thermoneutral voltage).

2.1. Reduction of the Specific Energy Demand

Increased operating temperature leads to reduced Open-Circuit Voltage (OCV) and reduced kinetic losses due to improved reaction and transport kinetics. This results in a reduction of the cell voltage as shown in results from Garbe et al.[18] and reproduced hereunder in **Figure 2a**. A different membrane thickness mainly influences the ohmic region as observed from the different gradients for the same temperature level (above ≈0.5 A cm^{-2}). On the other hand, the higher temperature of 120 °C reduces the cell voltage also in the activation region at the lower end of current density. Section 3 below, related to thermodynamics and reaction kinetics, provides more detail on the theoretical background for this improvement. Notwithstanding the higher gas cross-over at ET resulting in a lower faradaic efficiency compared to operation at 60 °C (Figure 2b), the lower cell voltage also leads to a reduction of the specific energy demand (w_{H_2}) of the electrolyzer (Figure 2c). This is particularly evident following the minima points at a current density of ≈0.2 A cm^{-2}, after which the specific energy demand increases in a linear fashion to follow the same trend of the input power to the cell. One can also note the effect of low faradaic efficiency at current densities <0.2 A cm^{-2} on performance. The presented results involved a pressurized system to maintain the water in a liquid state. Operating in steam (at the same temperature but lower pressure) would have led to a lower reversible voltage and hence, a lower specific energy demand.

2.2. Improved Catalyst Utilization

Currently, PEM technology heavily relies on the use of platinum group metals (PGM) for its catalysts. Such materials are expensive and their scarcity is feared to possibly become a bottleneck to electrolyzer installations when going to large scale.[19,20] While it is possible to apply lower loadings or increasing the current

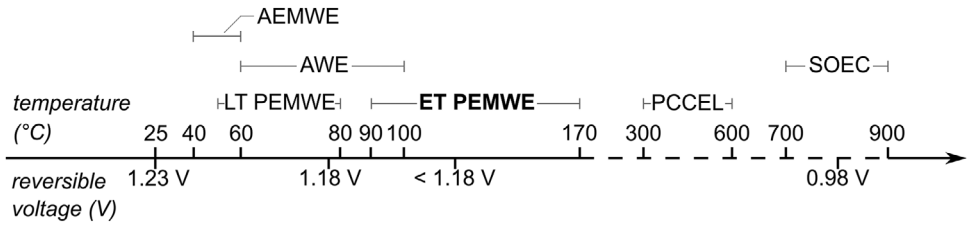

Figure 1. Operating PEM-based technology at ET would combine lower electrical power requirements with the advantages typically associated with LT PEMWE (numeric indicators not drawn to scale).

density, these techniques both result in increasing cell voltage.[21] Alternatively, support structures within the catalyst layers may be employed to improve catalyst distribution. Moreover, studies have looked into the optimal loadings for the most efficient use of catalyst.[21–23]

ET can potentially also contribute to improved catalyst utilization. However, a reduction in catalyst loading would lead to an increase in kinetic losses, canceling the savings made in lower voltages at ET. This would hence lead to operating at the cell voltages typical for LT. While it is then not possible to fully harvest the benefits of lower voltages and lower loadings at the same time, this would give the possibility to reduce PGM-based materials (at ET) and still have a performance, which would be at the same level as that currently achieved at LT (i.e., no 'relative' loss in performance). Ultimately, only a formal study would show the extent to which this interplay of cell performance, temperature and catalyst loadings can be beneficial to reduce PGM-based catalysts.

For the selection of proper catalyst materials at LT a strong volcano behavior of exchange current density and M-surface intermediate bond energy is reported in acidic and alkaline media for both cathodic Hydrogen Evolution Reaction (HER) and anodic Oxygen Evolution Reaction (OER),[24,25] as shown in **Figure 3**a,b. Hence, the optimal metals form not too strong and not too weak M-surface intermediate bonds. With the increase of reaction temperature in the ET PEMWE, the M-intermediate bonds become thermally activated and thus more reactive. Therefore, operating

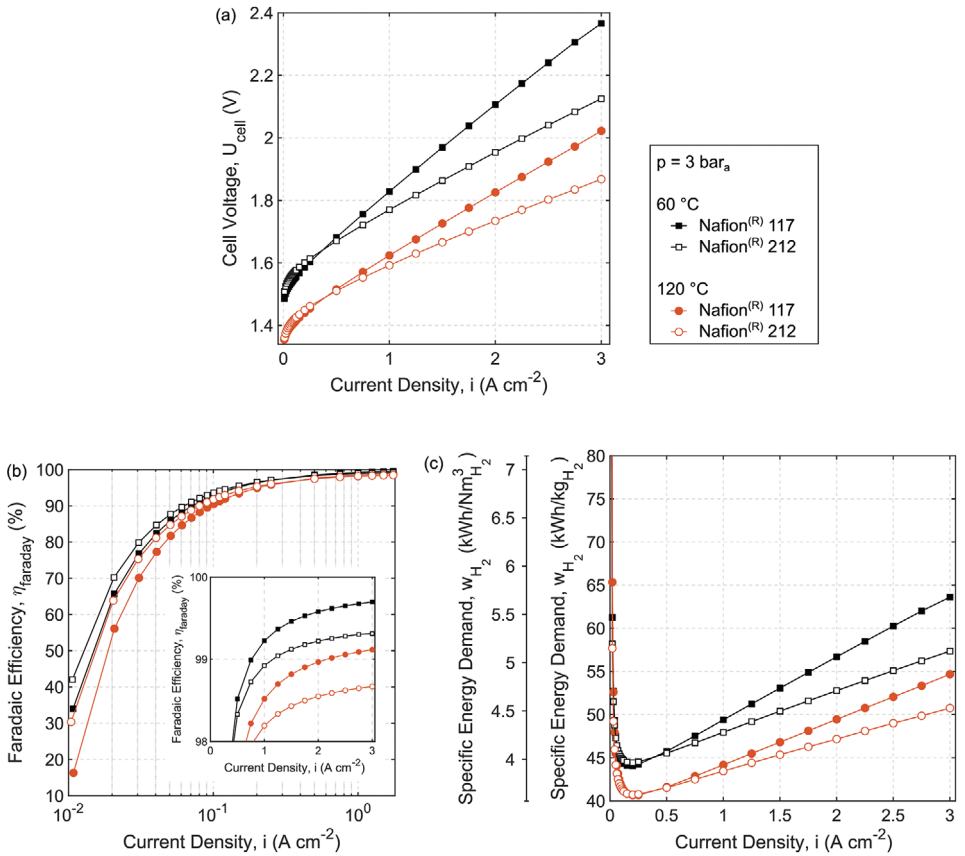

Figure 2. Comparison of LT and ET results with respect to a) polarization curves, b) faradaic efficiency (that in this case includes both hydrogen loss by permeation to the anode compartment and also by the electrochemical reaction of hydrogen and permeated oxygen on the cathode catalyst) and c) specific energy demand. (a) and (b) adapted with permission.[18] Copyright 2021, Elsevier.

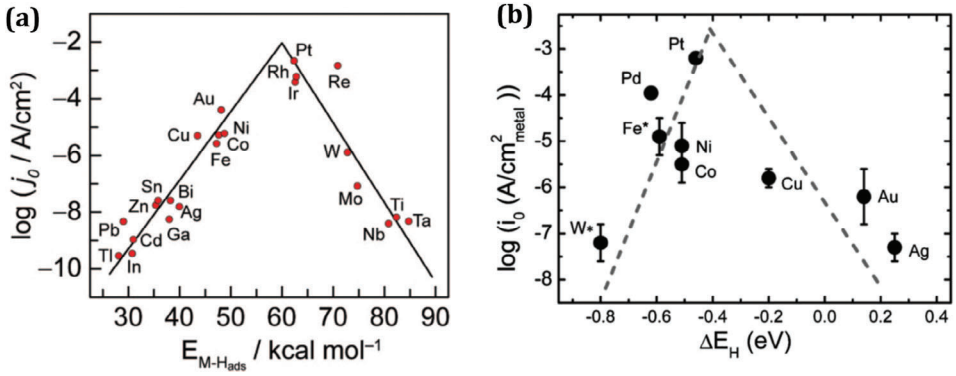

Figure 3. a) Exchange current density versus M—H bond energy for each respective metal surface in acidic media. Reproduced with permission.[24,26] Copyright 2010, American Chemical Society and Copyright 1972, Elsevier. b) Exchange current density versus M—H bond energy for each respective metal surface in alkaline media. Reproduced with permission.[25] Copyright 2013, The Royal Society of Chemistry.

at ET could widen the window of suitable catalyst towards less expensive elements that form at LT too strong M-intermediate bonds.

2.3. Thermal Management and Heat Integration

In exothermal operation, the cell voltage is higher than the thermoneutral voltage (U_{tn}) and excess heat needs to be removed from the cell to prevent it from overheating. The extent of heat loss from a PEMWE stack could be sufficiently significant to be recovered,[27] hence turning the waste energy into a resource. Possible heat recovery applications have already been identified at LT operation[28] and it is expected that higher temperatures would make the implementation of heat recovery more lucrative. In this regard, much can be learned from techniques suggested for fuel cell (FC) systems. This section, which has in fact been largely inspired by reviews summarizing heat recovery efforts in PEMFCs,[29,30] suggests four techniques to which ET PEMWE systems can be amalgamated to better make use of the waste energy. Efforts should also be directed at techniques of how the excess heat is extracted from the stack and transferred to the required fluid or planar surface.[28] It follows that significant research is yet required with regards to the inclusion of heat management strategies and assessment of their potential feasibility.

2.3.1. Heating Applications

The surplus heat energy from a PEMWE system could be utilized for hot water generation such as the scenario studied by Siecker et al.[31] In this case, a circulating fluid transfers the heat from the stack(s) to the hot water tank from which the required thermal loads are drawn (**Figure 4a**). When applied to FC systems, this technique has been shown to be even practical at the domestic level.[32]

2.3.2. Cooling Applications

Sorption cycles (Figure 4b) utilize heat sources to increase the refrigerant pressure in their cooling process instead of electric energy.[29] Sorption chillers reach lower coefficients of performance, but the fact that they can be driven by a waste heat compensates this fact.[33] Adsorption chillers, which utilize solid-vapor pairs, typically work best below 80 °C.[29] This makes them particularly interesting for applications using waste heat from an ET electrolyzer. Combined cooling, heating and power (CCHP or trigeneration) can thus be realized. As cooling is often much more needed than heating, this is an attractive option.

2.3.3. Power Generation

The Rankine cycle is a widely used power generation method, whereby steam produced in a boiler drives a turbine and generator for electricity generation. The water is then condensed back for recirculation. Organic Rankine cycles (ORCs) work on the same principle but adopt a low boiling point organic working fluid to recover waste heat from low-grade heat sources, with operating temperatures typically between 65 and 200 °C.[29] This advantage comes at the cost of lower efficiency, but ORCs are still attractive for producing electricity from waste heat. Figure 4c displays how heat recovery from PEMWE could be coupled to ORCs.

An alternative could be the utilization of the Seebeck effect. Herein, a voltage is generated when a temperature difference exists between the two sides of a thermoelectric generator (TEG)–Figure 4d. Such a technology is hailed for being silent, durable, scalable, compact, and having minimal operational costs due to wear and corrosion.[34] On the other hand, TEGs suffer from low efficiencies.[29]

It should be kept in mind that power generation from electrolysis waste heat means producing power within an electricity-consuming unit. The electricity should therefore rather be considered as a means of increasing efficiency of the electrolysis at high operation states.

2.4. Challenges for ET Operation and Measures for System Improvement

While ET may promise the advantages outlined above, much more is required to guarantee that operating in this temperature

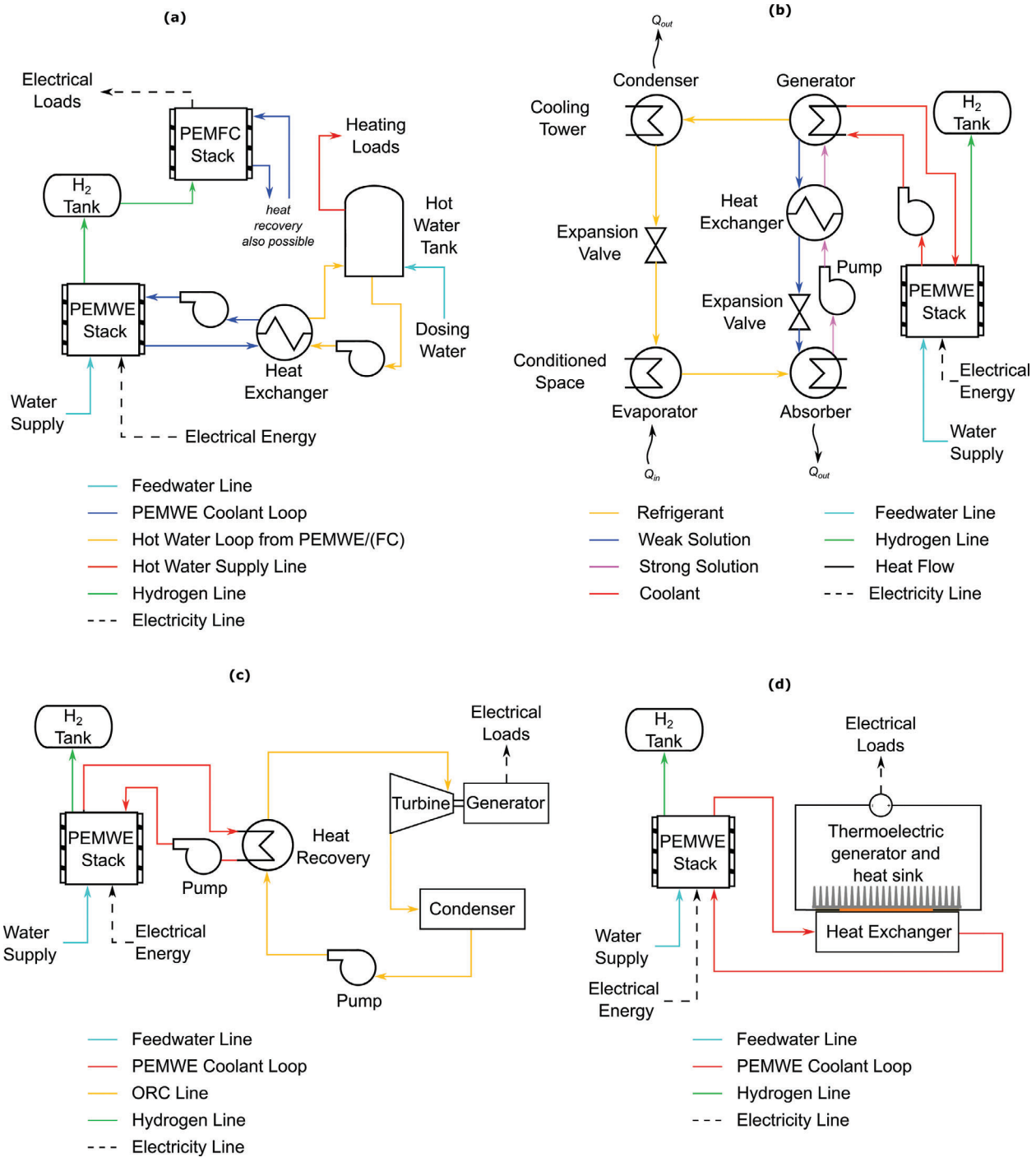

Figure 4. Schematic diagrams of heat management strategies in the recovery of waste energy from ET PEMWE systems–used for a) heating applications, b) cooling applications, c) power generation through the ORC, and d) thermoelectric generators. Inspired from the individual figures in Nguyen et al.[29] to make the case for PEMWE.

window would be a feasible alternative. In this regard, this section summarizes the key challenges which would definitely need to be addressed.

Naturally, ET PEMWE requires investigation of similar areas currently being studied also at LT such as optimum catalyst loadings[20,35,36] or even replacing Platinum Group Materials with non-precious electrocatalysts,[37,38] the reduction of gas cross-over,[39] modeling of species' transport,[40] stability and degradation,[41] pressurized operation,[42] the adoption of modern manufacturing approaches for porous structures' fabrication,[43] lower cost materials[44] and the influence of the Porous Transport Layer (PTL) properties.[45–48] In

the light of the research carried out to date, the following points are further considerations that would particularly apply for ET.

Membrane–Composite membranes seem to make up for the harsher conditions to guarantee suitable water retention, mechanical strength, and low gas cross-over. Though PEMWE typically requires relatively thick membranes to suppress hydrogen cross-over to an acceptable level, a thickness ranging down to 50 µm has also been tested at ET.[18] While benefiting from lower ohmic overpotentials, it is problematic to operate such a thin membrane in the lower end of current density (< 0.8 A cm^{-2} in the case of Garbe et al.)[18] due to the safety limit of 2% hydrogen in oxygen in the anode compartment. Moreover, chemical ionomer decomposition and irreversible structural changes of Perfluorosulfonic Acid (PFSA) membranes when subjected to ET call for alternative materials if PEMWE operation should have a suitable lifetime. Phosphoric acid (PA) doped polybenzimidazole (PBI) membranes have been utilized for steam conditions, albeit exhibiting a lower performance than membranes used for liquid water operation. Indeed, it is clear that there is a need still for the development of polymer electrolyte membranes with improved thermal, mechanical and chemical stabilities at ET.[49] Corti[50] suggests to explore membranes involving electrospun nanofibers to achieve high proton conductivity while reducing fabrication costs. It follows that the choice of ionomer in the catalyst layer must also satisfy the same requirements set for the membrane.

Catalyst–The majority of studies dealing with ET have looked into directions other than novel catalysts, typically resorting to those adopted at LT, or at most, their efficient utilization. The search for alternative catalysts, however, goes beyond the drive to reduce PGM materials due to their cost and availability. Indeed, catalyst activity,[51] electrolyte compatibility,[52] and stability[53] (shown to also change as a function of temperature) would also be factors to consider in catalyst selection. One may argue not to expect significant changes in the catalyst properties given the temperature is not substantially increased. Nonetheless, the cases outlined above did result in observable changes and may hence be seen as a possibility for finding improved catalysts in the ET operation window.

PTL–PTL optimization efforts (on porosity, thickness, texture, and pore diameter for instance) differ on whether water electrolysis is performed at atmospheric pressure or at higher pressures.[54] At ET, changes to the volumetric gas production rates[18] are expected to exert a direct influence on the mass transfer of reactants and products. This has been investigated experimentally by Li et al.[55] but the studied temperature was in this case limited to 100 °C. The experimental approach would need to correlate PTL properties (following a detailed characterization) to the respective electrochemical performance.[46,56] Acknowledging the greater challenge due to the harsher conditions, high-resolution visualization techniques can also be employed to aid the understanding of water/gas distribution in the porous media.[57,58] Such data would even serve as a basis for the development of mathematical models specifically catered for operation at ET.

Also related to the PTL is an improved material choice to withstand increased passivation at ET.[59] A number of options exist to replace titanium by other metals plus corrosion-resistant coatings.

Bipolar Plate (BPP)–The material issue just described is even more severe for the BPP which involves more mass. One would have to assess however whether the coating cost would cancel any savings from lower catalyst loadings.[53] This is particularly relevant as these components can constitute a substantial proportion of the stack cost–approximately up to two-thirds for a LT setup.[19]

Reactant Operating Phase–Possibly, ET PEMWE could be operated with steam instead of liquid water. On the one hand, this could simplify mass transport in the electrolyzer as both reactant and product phase would be gaseous. Increasing temperature and gas pressure could increase the number of interactions of the water molecules with the active centers per time and area. On the other hand, liquid phase operation means higher water activity at the active catalyst sites compared to gaseous operation. Therefore, it is very difficult to be sure about the outcome of such a change in the system. There are only very limited works focusing on this specific topic and operating in steam in PEMWE: vapor-fed PEMWE has been mainly studied with water vapor from a humidified carrier gas, at temperatures well below 100 °C. Spurgeon and Lewis[60] opted for vapor operation specifically to mitigate mass transport limitations associated with bubble formation. Results indicated that at a current density below 40 mA·cm^{-2}, a more favorable performance was observed with water vapor over liquid operation. Above this limit, however, mass flux of water to the PEM limited the electrolysis performance with the use of water vapor. Improved performance (with water vapor) was also observed by Schuler et al.[61] The current densities employed were also on the lower end, (<100 mA·cm^{-2}), since the focus of the study involved the characterization of the reaction mechanism for the OER for LT PEMWE. Here, the authors suggested that when in contact with liquid water, the ionomer swells in a way as to distort the electrical percolation network in the catalyst layer. Consideration should also be given to diffusion/convection flow coefficients and to the fact of having an activity other than unity (as typically used for liquid water). Indeed, limited data is available on the effect of using different phases in PEMWE at ET.

Operating parameters and system components–While cell clamping pressure is instrumental to limit interfacial resistance and hence ensure a good electrical conductivity, excessively high values may lead to damage of the components, reduced PTL porosity and loss of proton conductivity.[62,63] Identifying optimal clamping pressures becomes particularly important at ET where membrane swelling is more pronounced, and may possibly further increase any overpressure. More studies are also required at a system level and the ancillaries, which would be required to provide the harsher operation conditions. For instance, ion-exchange resins are typically used to guarantee an adequate purity of the circulated liquid water. These components however are typically restricted to LT.[19] Alternatives such as resin materials capable of withstanding ET, different treatment techniques or system modifications involving partial purification must hence be sought and studied.

Effect of heat recovery and utilization–A number of studies have already looked into integrated energy systems involving LT PEMWE.[64–69] This can also be extended to ET[70] and incorporate

heat utilization for secondary purposes such as, but not limited to, the examples outlined above.

Techno-economic analyses–In continuation to the latter point, hydrogen economics[71] would also need to be considered apart from the technical feasibility and efficiency standpoint. Cost-effectiveness studies may tackle different facets of the technology such as i) the catalyst loading reduction potential by weighing performance changes and cost at various loadings, ii) the effect of opting for more corrosion-resistant materials such as tantalum over titanium, iii) consideration for additional costs (with respect to Capital and Operational Expenditures) of Balance-of-Plant (BoP) components needing to operate in harsher conditions, iv) how the system would perform and deal with start/stop situations (due to the intermittency of power sources), or v) whether efficiency gains would translate to monetary savings, and to what extent.

2.5. Review Scope, Structure, and Delimitations

Many areas of research have been identified so as to make hydrogen production more competitive[19,72] with temperature expected to be one of the factors worth exploring to improve performance.[73,74]

The interest in opting for ET operation is confirmed by a recent review by Zhang et al.,[16] and Corti.[50] In the former,[16] the merits and challenges of water electrolyzers at ET are discussed both for the established technologies of AWE and PEMWE and also for the more novel techniques. It also addresses the material selection for the different cell layers, especially with regard to membranes and electrocatalysts. Moreover, it makes reference to the general performance and stability for ET systems. In the case of Corti,[50] the study focused on PEMWE and critically assessed polymer electrolytes employed for ET, in particular by their comparison to LT operation. While acknowledging that direct comparison is not easy due to differences in the additional materials making up the cell assembly, the author suggests that a better trend is observed for LT results and it is not clear that ET operation poses any clear advantage.

The presented review focuses solely on PEMWE, but does not solely consider membrane materials. In particular, it delves deep into full-cell studies and mathematical modeling considered at ET operation. In the case of full-cell studies, these are used as a base to describe and critically assess the different components from cell to a system level. The individual details from these studies are hence structured to provide a holistic view of the state-of-the-art for the respective cell or system component.

Having already highlighted the advantages and challenges of PEMWE operated at ET, the review follows by first presenting the theoretical basis of thermodynamics and reaction kinetics, which make ET more favorable. The materials considered for each component of a PEMWE setup at ET are then discussed. The final section looks at system performance from a higher perspective with respect to input power, operating phase utilized, results from mathematical modeling and how ET affects degradation. This review is hence expected to set the stage for future studies and hence allow for a broadly informed decision of ET PEMWE for different applications.

3. Thermodynamics and Reaction Kinetics of ET PEMWE

The reduction of cell voltage when operating PEMWE at higher temperatures is a result of i) reduced Open-Circuit Voltage (OCV) and ii) reduced kinetic losses from improved reaction and transport kinetics. This section is intended i) to present the underlying theory so as to outline how the improvements with ET are brought about and ii) as a guide to compute the relevant voltages to be expected at ET.

3.1. Cell at Open Circuit Conditions

The electrochemical splitting of water in standard conditions (298 K, 1 bar) occurs as follows:

$$H_2O_{(l)} \rightarrow H_2(g) + \frac{1}{2}O_2(g) \tag{1}$$

Energy needs to be supplied to the system for the reaction to occur. Applying the First Law of Thermodynamics to the electrolyzer with a steady flow of heat and work (in the form of electrical power) and assuming changes in height and potential energy being negligible:

$$0 = U_{\text{cell}} \cdot I + \dot{Q} - \frac{I}{nF} \cdot \Delta_R h(T,p) \tag{2}$$

where U_{cell} is the applied voltage, I is the applied current, $\dot{Q}$ is the heating power, n is the number of electrons exchanged in the reaction, F is the Faraday constant and $\Delta_R h$ is the change in specific enthalpy h as a function of temperature T and pressure p.

Moreover, also applying the Second Law of Thermodynamics for the Electrolyzer:

$$0 = \frac{\dot{Q}}{T} - \frac{I}{nF} \cdot \Delta_R s(T,p) + \dot{S}_{\text{irr}} \tag{3}$$

where $\Delta_R s(T,p)$ is the change in specific entropy as a function of temperature and pressure and $\dot{S}_{irr}$ is the entropy generated within the system by the irreversibility of the process.

For the open-circuit condition, we have reversible operation (i.e. $\dot{S}_{irr} = 0$) and from Equations (2) and (3):

$$U_{\text{rev}} = -\frac{1}{nF} \cdot \left(T\Delta_R s(T,p) - \Delta_R h(T,p)\right) \tag{4}$$

$$\dot{Q}_{\text{rev}} = \frac{I}{nF} \cdot T\Delta_R s(T,p) \tag{5}$$

where U_{rev} is the reversible voltage and $\dot{Q}_{\text{rev}}$ is the heat energy input under reversible conditions.

From the definition of the Gibbs free energy, $\Delta_R g = \Delta_R h - T\Delta_R s$, and comparison to Equation (4), the following is obtained:

$$U_{\text{rev}} = \frac{\Delta_R g(T,p)}{nF} \tag{6}$$

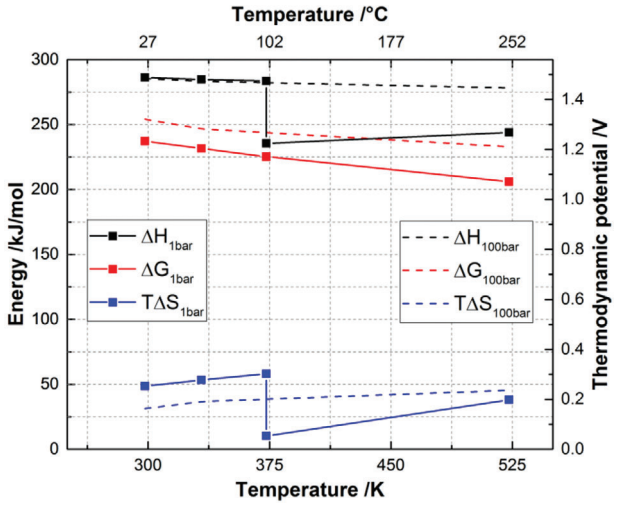

Figure 5. The variation of the energy components required to split water as a function of temperature at 1 bar and 100 bar. Reproduced under terms of the CC-BY license.[19] Copyright 2017, The Authors, published by The Electrochemical Society.

The enthalpy and entropy changes for the computation of the Gibbs free energy can be calculated from the elementary properties of each constituent in the reaction:

$$\Delta_R h\ (T, 1\ bar) = \Delta h^f_{H_2} + (0.5) \cdot \Delta h^f_{O_2} - \Delta h^f_{H_2O} \tag{7}$$

$$\Delta_R s\ (T, 1\ bar) = s_{H_2} + (0.5) \cdot s_{O_2} - s_{H_2O} \tag{8}$$

where Δh^f and s refer to the temperature-dependent values of enthalpy of formation and entropy for O_2, H_2, and H_2O at $p = 1\ bar$, respectively, and can be found in data tables.[75,76] Equation (6) can then be used to respectively compute the reversible voltage. **Figure 5** displays the effect of elevated temperature on $\Delta_R g$, $T\Delta_R s$ and $\Delta_R h$. The decrease in $\Delta_R g$ with increasing temperature effectively means a lower U_{rev}, which in turn signifies that a lower electric power input would be required.

Applying increased pressure improves the storage density of hydrogen. This has an effect on $\Delta_R g(T,p)$ and leads to higher U_{rev}. The reader is referred to Hanke–Rauschenbach et al.[77] for details on how these can be calculated for increased pressure. From an operational point of view, it should be noted that higher system pressure also increases the water saturation temperature such that the system may operate with water in the liquid state even above 100 °C.

3.2. Cell at Load Conditions

Under load conditions, a higher cell voltage than U_{rev} needs to be applied to produce hydrogen:

$$U_{cell} = U_{rev} + U_{loss} \tag{9}$$

where U_{loss} sums up the contributions of various voltage losses arising from i) reaction kinetics due to the charge transfer processes at the electrode/electrolyte interfaces, ii) charge transport within the bulk media and at the individual interfaces of the cell components, and iii) mass transport of the reactants and products towards and away from the active (surface) area.[42,78]

An important variable to evaluate the cell under load conditions is the so-called thermoneutral cell voltage (U_{tn}). This can be derived by setting $\dot{Q} = 0$ in Equation (2):

$$0 = U_{tn} \cdot I + 0 - \frac{I}{nF} \cdot \Delta_R h\,(T,p) \tag{10}$$

$$U_{tn} = \frac{\Delta_R h\,(T,p)}{nF} \tag{11}$$

The entropy generation term $\dot{S}_{irr}$ can be defined as:

$$\dot{S}_{irr} = \frac{I \cdot \left(U_{cell} - U_{rev}\right)}{T} \tag{12}$$

And inserted in Equation (3), we obtain:

$$\dot{Q} = \frac{I}{nF} \cdot T\Delta_R s\,(T,p) - I \cdot \left(U_{cell} - U_{rev}\right) \tag{13}$$

For $\dot{Q} = 0$ and $U_{cell} = U_{tn}$ we deduce that:

$$0 = \frac{I}{nF} \cdot \Delta_R s\,(T,p) - \frac{I \cdot \left(U_{tn} - U_{rev}\right)}{T} \tag{14}$$

And following re-arrangement:

$$U_{tn} - U_{rev} = \frac{T\Delta_R s\,(T,p)}{nF} \tag{15}$$

Given this result, Equation (13) can be re-formulated such that:

$$\dot{Q} = I \cdot \left(U_{tn} - U_{cell}\right) \tag{16}$$

Equation (16) shows that $\dot{Q} > 0$ (heat needs to be supplied) if $U_{cell} < U_{tn}$ while $\dot{Q} < 0$ (heat needs to be removed) if $U_{cell} > U_{tn}$. This is particularly relevant for ET operation where the higher-grade waste heat (when compared to LT) would make heat recovery more advantageous. In this regard, Section 2.3 suggested possible uses to integrate the waste heat to improve the overall performance of the system.

As follows from Equation (11), the dependence of U_{tn} on temperature can be traced to the variation of $\Delta_R h(T,p)$ in Figure 5. The sudden drop observed in the figure occurs at the boiling temperature of water (for 1 bar_{abs} in this case) and makes up for the latent heat of vaporization required for the change of state from liquid to steam. This change is shifted to higher temperatures when operating at an increased pressure.

3.3. Performance Metrics for ET PEMWE

Multiple metrics have been utilized for assessing the performance of PEMWEs,[79] making comparisons of different systems a non-trivial task. A simple and practical measure to assess performance would involve the specific energy demand (w_{H_2}). In the

case of exothermal operation when heat needs to be removed, the specific energy demand of the electrolyzer can be defined as:

$$w_{H_2} = \frac{P_{el}}{\dot{n}_{H_2}} \tag{17}$$

where $\dot{n}_{H_2}$ is the molar flow of hydrogen and P_{el} is the supplied electrical power, such that:

$$w_{H_2} = \frac{U_{cell} \cdot I}{\dot{n}_{H_2}} \tag{18}$$

It is convenient to express $\dot{n}_{H_2}$ as:

$$\dot{n}_{H_2} = \eta_{faraday} \cdot \frac{I}{2F} \tag{19}$$

where $\eta_{faraday}$ is the Faradaic efficiency, which takes into account the possible loss of a fraction of reaction products[80] such as due to gas cross-over.

Hence:

$$w_{H_2} = \frac{2F \cdot U_{cell}}{\eta_{faraday}} = \frac{2F \cdot \left(U_{rev} + U_{loss}\right)}{\eta_{faraday}} \tag{20}$$

Equation (20) was used to develop Figure 2c and highlight the effect of the respective parameters on system performance. The effect of temperature to drive down the specific energy demand of the system can be clearly observed.

In the case of endothermal operation, the additional effort for heat supply has to be considered, such that:

$$w_{H_2} = \frac{U_{cell} \cdot I + \dot{Q}}{\dot{n}_{H_2}} \tag{21}$$

On a system level, which needs to also take into account balance-of-plant (BOP) components, w_{H_2} for exothermal operation would involve:

$$w_{H_2} = \frac{P_{el}^{stack} + P^{BOP} + \dot{Q}^{BOP}}{\dot{n}_{H_2}} \tag{22}$$

where P_{el}^{stack} is the electrical power input to the stack, P^{BOP} is the electrical power input to the BOP components (such as pumps) and $\dot{Q}^{BOP}$ is the heating power input to the BOP components (such as for heating the dosing water to make up for the water consumed in the reaction).

In the case of endothermal operation on a system level, the heat supplied to the stack ($\dot{Q}^{stack}$) would also need to be taken into account:

$$w_{H_2} = \frac{P_{el}^{stack} + \dot{Q}^{stack} + P^{BOP} + \dot{Q}^{BOP}}{\dot{n}_{H_2}} \tag{23}$$

Some authors prefer to refer w_{H_2} to a reference value and by this means introduce an efficiency (ϵ). Typical reference values are the reversible energy required for the water-splitting

$$w_{H_2}^{rev} = \Delta_R g\,(T, p) \tag{24}$$

or the higher or lower heating value of hydrogen, HHV, and LHV, leading to the following exemplary definitions:

$$\epsilon = \frac{w_{H_2}^{rev}}{w_{H_2}} \tag{25}$$

$$\epsilon_{HHV} = \frac{HHV}{w_{H_2}} \tag{26}$$

$$\epsilon_{LHV} = \frac{LHV}{w_{H_2}} \tag{27}$$

In the latter efficiency definitions, the LHV and HHV help in setting the effort of the work input (i.e. electrical energy provided) in relation to the energetic value of the product in its subsequent utilization, by either considering (HHV) or neglecting (LHV) the contribution of the condensing enthalpy of water (equal to 44 $kJ\ \ mol^{-1}$ at 25 °C).

4. Evaluation of Materials and Components for ET Operation

Operation at ET maintains the same cell structure as present in classical LT PEMWE. The membrane separating the reaction products is in contact with a catalyst layer on either side. Porous transport layers are required to gradually change the pore size: from the nanometer-sized catalyst particles in the catalyst layer to the millimeter-sized flow field channels, through which reactants are supplied and products removed. The schematic in **Figure 6** shows the positioning of these functional layers, and summarizes the main materials that have been employed in full-cell tests at ET operation. A description of the considered materials is given in the following sections.

4.1. Membrane

The membrane is sandwiched between the two gas diffusion electrodes to support ionic current while preventing electronic contact and cross-over of the evolved gases.[81] At LT, the commercially available polymer electrolyte membrane Nafion® has been the typical choice due to its excellent chemical and thermal stability, mechanical strength, and high proton conductivity.[82]

This section summarizes membrane materials that have been subjected to polarization experiments at ET operation until now. It should be however noted that other materials have been suggested to be possibly suited for ET–the reader is referred to more comprehensive membrane reviews for further details.[16,50,81,83] The effect of membrane material/type, thickness, doping, blending and additive manufacturing on the performance and stability (chemically, mechanically, hydration) at different ET operating conditions (steam or liquid) are summarized in the next sections.

Early investigations for suitable membranes at ET involved sulfonated poly(arylene ether ketone) (SPEEK), sulfonated poly(arylene ether sulfone) (SPES), sulfonated poly(phenyl quinoxaline)s (SPPQ), and sulfonated polybenzimidazole (SPBI).[84] SPPQ was the only one to compare favorably with Nafion with regard to thermal stability. Electrolysis cell testing was only performed on SPEEK but temperatures had to

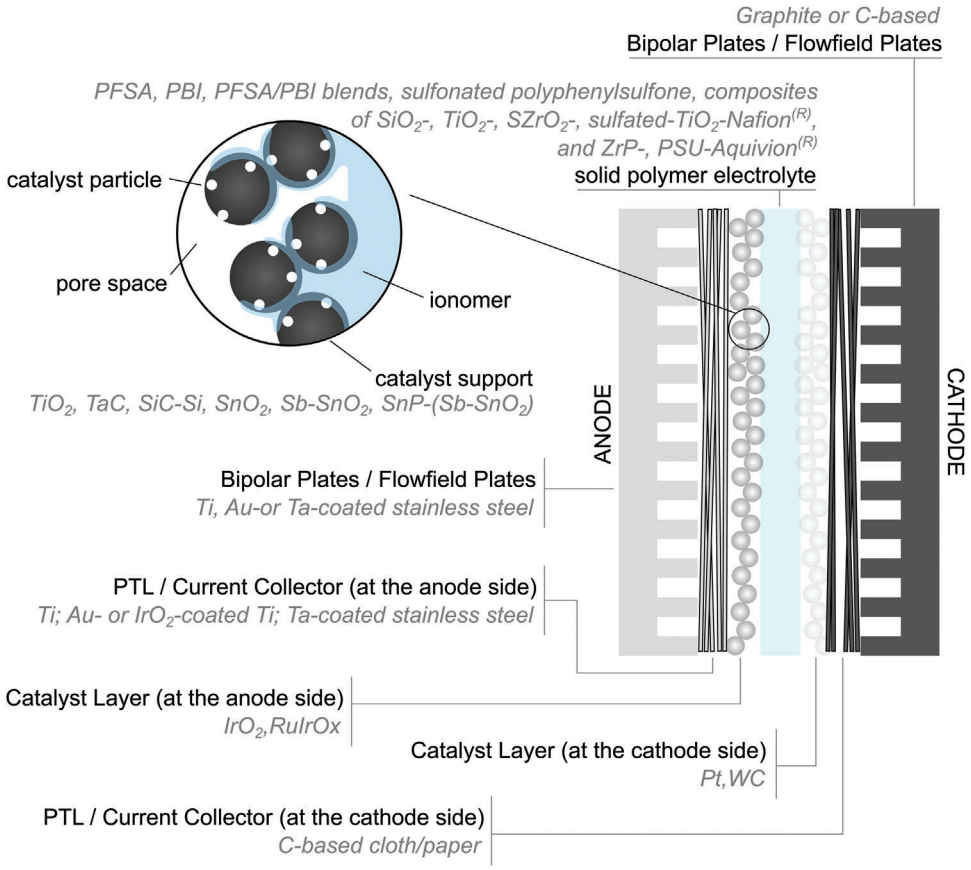

Figure 6. Schematic cross-section showing the main components making up a PEMWE cell and compiling the materials that have been considered and studied for ET operation. Complete details and respective references given in the main text.

be limited to 60 °C due to the material being prone to creep with increasing temperature (and hence not suitable for ET operation).

4.1.1. Perfluorosulfonic Acid (PFSA) Based Membranes

PFSA membranes constitute a hydrophobic, perfluorinated backbone structure for stability, equipped with sulfonic acid ($SO_3^- H^+$) terminated side chains to provide proton conductivity following hydration. In LT, such membranes promise a reliable and stable operation and their use has been extended for ET operation, too. Long-side-chain (LSC) PFSA Nafion ionomers with Equivalent Weights (EW) ranging between 900 and 1100 g of polymer per mole of fixed charges (g mol^{-1}) were considered in multiple studies–namely Nafion 115,[49,85–87] Nafion 117[55,88] and Nafion 212.[18,89] Ito et al.[90] investigated the intrinsic properties of Nafion 117 membranes when operated under PEM water electrolysis conditions (in liquid state). Both the *water uptake* (WU) and *proton conductivity* were observed to increase with temperature for the studied range up to ≈120 °C. However, the employed pre-treatment technique (such as drying temperature) seems to exert an influence on these properties.[90,91] It follows that a higher water uptake leads to increased *membrane swelling*, as also measured by Mališ et al.[92] and Gebel et al.[93] **Table 1** summarizes some of these key properties as a function of temperature.

Another PFSA polymer that has been considered is Aquivion.[95] Compared with Nafion, Aquivion has shorter side chains and a higher degree of crystallinity, which allows for lower equivalent weights without compromising mechanical stability. Water sorption has been observed to increase with a decrease in EW due to the increase in acid sites for sorption.[96] Besides improved mechanical properties and a higher glass transition temperature,[97] proton conductivity for the short-side-chain (SSC) Aquivion E87-12S has been shown to improve over LSC PFSA when tested up to 120 °C at 95% relative humidity.[98]

Effect of ET on PFSA Membranes: Kim et al.[49] investigated the effect of temperature on PFSA membranes using Small Angle X-Ray Scattering (SAXS). The polymer crystal structure was observed to change with steam above 120 °C and did not recover its original structure when the temperature was decreased from 150 to 30 °C. Even though the membrane conductivity increased monotonically with temperature, the authors suggested that the structural change could possibly explain the drop in membrane conductivity over time. This was also observed with an Aquivion membrane, which already has a comparably high apparent glass transition temperature within the PFSA group.

A similar loss in performance also occurred in a pressurized system with the membrane operating in liquid water.[92] When

Table 1. Properties of Nafion 117 membrane immersed in liquid water. Adapted with permission.[90,94] Copyright 2011, Elsevier and 1985, The Electrochemical Society and IOP Publishing. All rights reserved.

Immersed water temperature [°C]	Water content[a], ω [wt%]	Water content[b], λ [mol H_2O/ mol SO_3]	Wet thickness [μm]	Swelling ratio in through-plane, [%]
Dry	1.7	1.0	185	-
100	35	21.4	220	18.9
140	50	30.5	237	28.1
170	102	62.3	265	43.2

[a] Water uptake is expressed as $\omega = (w_{wet} - w_{dry})/w_{dry}$ where w_{wet} and w_{dry} respectively refer to the weight of the wet and dry samples; [b] Alternatively, water uptake can also be represented by the number of water molecules per sulfonic acid site and is given by $\lambda = (\omega \cdot EW)/M_{H_2O}$ where EW is the equivalent weight for Nafion and M_{H_2O} is the molar weight of water.

measured at a fixed voltage, the current density noticeably decreased with time (when studied at 110, 130, and 150 °C over a time-frame of ≈600 h). The trend reflected the change in proton conductivity, characterized by an initial exponential drop followed by a slow linear decline for temperatures of 130 and 150 °C. Mališ et al.[92] identified two swelling phases explaining this behavior. The first leading to a restructuring of the hydrophilic domains causing increased ionic mobility, followed by a second phase responsible for irreversible changes in the internal structure of the polymer material, that is, a loss of interaction between the polymer backbone chains, with operation exceeding the apparent glass transition temperature (T_g) expected to trigger the latter phase. It should be noted that this distinction at T_g also brings about a change in the activation energy value in Arrhenius plots.[99] Low T_g (with respect to the operation window considered for ET) is characteristic for conventional PFSAs.[74]

Non-Fluorinated Membranes: In view of the limited mechanical stability of fluorinated electrolyte membranes at ET, Kim and Ohira[100] studied cross-linked sulfonated polyphenylsulfone (CSPPSU) material as an alternative. In this case, the stabilities were assessed by placing the membranes in water at 85 °C and in an autoclave at 150 °C for a prolonged period of time and compared the ion-exchange capacity (IEC), WU, and conductivity before and after the test period. Comparable values were interpreted as satisfactory stability. Moreover, the polymer structures did not indicate any structural change at the nm length scale when observed under SAXS. On the other hand, the electrochemical performance was lower than that achieved with Nafion.

Use of Thinner Membranes: As opposed to the thin membranes used in PEMFCs (≈12 μm), thicker membranes are employed in PEMWE to reduce hydrogen cross-over.[50] On the other hand, the use of thinner membranes (such as 50 μm) decreases the ohmic overpotential and in turn, improves the electrical efficiency.[18] Interestingly, the decrease in interfacial resistance is not as pronounced as for thicker membranes as the greater degree of swelling in the latter is expected to increase more the compression of the catalyst layer toward the PTL. On the downside, the thinner membrane facilitates gas cross-over, and based on the safety limit of 2% hydrogen in oxygen in the anode compartment, the minimum current density at which the system can be operated increases from 0.36 A cm^{-2} (at 60 °C for a 180 μm membrane thickness) to 0.76 A·cm^{-2} (at 120 °C for a 50 μm membrane thickness).[18]

4.1.2. Phosphoric Acid (PA)-Doped Membranes

Aili et al.[101] studied PA-doped membranes based on Nafion, PBI, and their blends in a steam environment at 130 °C. While the cell based on PA-doped PBI suffered from severe membrane degradation, the cells equipped with PA-doped Nafion showed better performance stability. The Nafion-based membrane displayed a higher ohmic overpotential than with the membrane made of PBI. The poorer performance was blamed on a larger membrane electrode interfacial contact resistance and uneven current distribution, possibly arising from limited dimensional stability.[102] (In this case, a Nafion dispersion and PBI were used in the preparation of the anode and cathode electrodes, respectively). By further catalyst and electrode optimization, the performance was further improved.[103,104] It was later shown that it is essential to keep the membrane fully humidified when polarized, to avoid PA redistribution and leakage triggered by migration of protonated PA cations.[105] The presence of PA may also be problematic with respect to corrosion of construction materials for the cell hardware.[106]

Blend membranes have in general been shown to improve mechanical strength and chemical stability in fuel cell (FC) performance.[101] When applied to PEMWE using steam, such membranes, however, offered considerably lower proton conductivity than the pure PA-doped Nafion or PBI. For this reason, no further electrolysis cell tests were performed on this binary alternative.

PA-doped PBI has been shown to offer a better conductivity than PA-doped Nafion. On the other hand, the former suffers from durability problems.[101] In the case of a liquid medium, Skulimowska et al.[98] assessed sulfonated ether-linked polybenzimidazole poly-[(1-(4,40-diphenylether)-5-oxybenzimidazole)-benzimidazole] (PBI-OO). While acknowledging that the PBI-based alternative did not perform as good as a sulfonated PFSA membrane, the authors of the respective study did not dismiss sulfonated polybenzimidazole as a lower-cost alternative to PFSA membranes for water electrolysis.

4.1.3. Composite Membranes

Another approach to improve the properties of a membrane besides adopting a different or modified polymer structure involves the introduction of additives. Membrane hydration, mechanical

reinforcement and gas cross-over are properties, which are influenced by such filler materials.

Membrane Hydration: Membranes are expected to be more prone to dehydration at elevated temperatures, and since conductivity depends on water content this results in a higher ohmic overpotential.[85,88] In the case of fuel cells, this effect has been mitigated with the use of composite membranes containing hygroscopic ceramic oxide fillers to harness the water retention properties of these materials and also to provide additional acidic sites, which in turn increase the concentration of mobile protons.[107,108] It should however be noted that the ion-exchange capacity of doped membranes, representing the number of fixed charges in an ion-exchange polymer relative to its weight, was in some cases measured to be less than the undoped case.[109,110] This was attributed to the increased density of the composite sample due to the ceramic powder. Nonetheless, actual water uptake measurements in the latter studies always favored the doped membranes.

The addition of inorganic fillers was also applied to electrolysis, with the use of BPO_{4-},[111] SiO_{2-},[85] TiO_{2-},[86] $SZrO_{2-}$[87] and sulfated-TiO_{2-}[109] Nafion composites exhibiting an improved performance to commercial additive-free Nafion. While acknowledging these benefits, Ghassemzadeh et al.[112] exert caution with the filler content, as any excess may have a negative effect on the proton mobility and hence on conductivity. This could possibly explain the large discrepancy in conductivity values measured by Xu et al.,[113] between a commercial perfluorinated polymer-silica composite membrane and Nafion. The optimum content must be determined with consideration to membrane preparation method, size and surface properties of the particles. Moreover, imperfections in the surface morphology involving agglomerates of filler (observed on the microscopic scale) have resulted in sub-optimal performance.[87] Skulimowska et al.[98] also studied a SSC Aquivion membrane-based composite involving ZrP as the inorganic filler. An increased ohmic resistance contribution was observed from in situ water electrolysis tests when compared to the additive-free membrane–found consistent with the ex situ measurement of lower proton conductivity.

Mechanical Strength: The membrane is subject to multiple sources of mechanical stress, which may arise due to non-uniform stress distribution at the channel/bipolar plate interface, thermal cycling, or the growth of voids with changing water vapor pressures.[114] The mechanical properties of the membrane hence become important to avoid the formation of pinholes, delamination of the membrane electrode interfaces, and cracks which would drastically increase gas cross-over and possibly leading to unsafe hydrogen in oxygen mixture levels. The requirement of durable membranes is further amplified in the pursuit of thinner membranes to reduce ohmic resistance. Giancola et al.[115] have studied poly(arylene ether sulfone) (PSU) fiber webs as reinforcement to SSC Aquivion membrane. Unless the reinforcement is not too high as to reduce the concentration of charge carriers, the composite membrane was found to be a good compromise between high mechanical strength and a proton conductivity resulting in minimal changes in MEA electrochemical performance. The reinforcement was also found to result in lower swelling, and hence improved dimensional stability.

4.1.4. Proton Conductivity

Having a determining role in PEMWE performance, especially in the case of ohmic overpotenials, this section collectively looks at the conductivities obtained for some of the membranes highlighted above. A number of studies already looked at proton conductivity of Nafion[116–118] and PBI.[119,120] These were, however, performed in a humidified atmosphere in a relevant range to simulate fuel cell operating conditions and may therefore not represent electrolysis conditions correctly.[92] Indeed, contrasting performances were obtained when working in a 100% Relative Humidity (RH) atmosphere[121] or with lower intermediate values of RH.[118,122]

Figure 7a summarizes proton conductivities of membranes intended for a WE environment. The legend of the figure highlights measurement protocol details involving level of hydration and pressure. A distinction is made on whether the in-plane or through-plane results were given, even though no significant difference between the two measurements is to be expected unless the material morphology varies noticeably in different directions,[115,121,123] such as with the introduction of a reinforcement layer.[124] In general, it is observed that for the studied conditions, conductivity always increased with temperature. The highest membrane conductivities were obtained when operating in full hydration (i.e. fully immersed in liquid water).[92,125,126] With regards to composite membranes, Skulimowska et al.[98] reported lower conductivity with a ZrP-based additive in a SSC PFSA membrane. On the other hand, High- Frequency Resistance (HFR) measurements with SiO_2, TiO_2, $SZrO_2$ and S-TiO_2-Nafion based membranes offered a lower ohmic resistance (compared to the pure Nafion), which in turn resulted in lower operating voltages. In the case of PBI, the effect of lower performance will be made more clear in the section related to the *Performance of ET PEMWE*. The highest conductivity at ET was reported by Mališ et al.[92] for Nafion 117. Unfortunately, this improvement is short-lived since conductivity drops substantially with time at ET (Figure 7b), with pressure having a significant role in this case. Further assessing the results by generating Arrhenius' plots showed two distinct conductivity domains (Figure 7c), with the change occurring in the temperature ranges between 90 and 110 °C. Extending the discussion already presented in Section 4.1.1, the onset of plasticity at the apparent glass transition temperature induces a structural change that is considered as the reason for the change in conductivity, and irreversible upon lowering the temperature.[49]

4.2. Catalysts and Catalyst Layers

As typically adopted for LT conditions, IrOx and Pt were the most common catalysts employed at the anode and cathode, respectively, at ET conditions.[22,55,89,92,98,101,102,127] In general, these materials have both high catalytic activity and electrical conductivity while being relatively stable against corrosion. However, while temperature improves reaction kinetics, the OER rate may be slowed down by the choice of electrolyte such as the case of PBI membranes leading to phosphate adsorption on iridium oxide.[52,128] Moreover, crystallite size of the IrO_2 was found to have an impact on stability.[128]

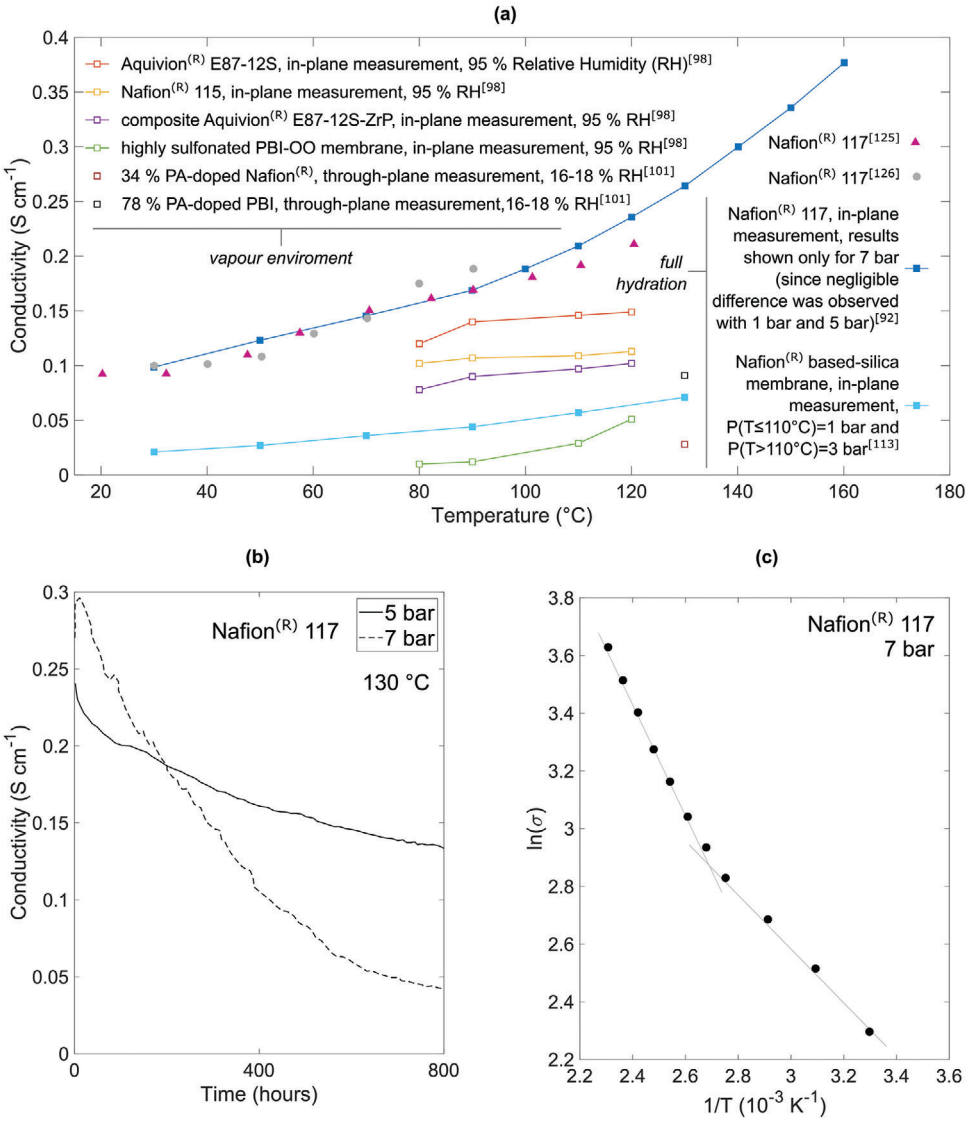

Figure 7. a) Collection of conductivity (σ) trends for ET with the legend highlighting the different measurement conditions. b) Variation of Nafion 117 conductivity with time at an operating temperature of 130 °C. Adapted with permission.[92] Copyright 2016, Elsevier. c) Arrhenius' plot for the conductivity at increased pressure. Adapted with permission.[92] Copyright 2016, Elsevier.

The overvoltage for the OER is lower with RuO_2 than for IrO_2, but corrosion phenomena limit its use only in stabilized forms such as mixed oxides.[82,98,113,127] Variants such as RuIrOx were also considered to improve catalyst utilization due to their 3D microstructure.[95,109,113] However, the stability of Ru is below Ir stability, which limits its use in ET applications. Higher temperatures in aqueous environments are more demanding for metal oxide based catalysts due to deactivation by hydrothermal degradation. Operation at higher temperature has the potential to fasten the sluggish kinetics depending on the reaction mechanism. The OER can occur via the adsorbate evolution mechanism or the lattice oxygen mediated mechanism. Especially on Ir or Ru-oxide based catalysts, ET operation could shift the mechanism from the adsorbate evolution mechanism to the lattice oxygen mediated and hence could further improve the performance. Nevertheless, the optimum between hydrothermal degradation and improvement by lattice oxygen mediated has to be found.

With regards to the cathode, tungsten carbide (WC) was assessed for its suitability as a non-platinum hydrogen evolution reaction.[51] The catalytic activity of WC was found to drastically improve with increasing temperatures up to 150 °C. On the other hand, the activity of platinum was even observed to slightly decrease. Moreover, the synthesis route of WC has been shown to exert an effect on catalytic activity.[129] Also intended for steam operation and a PA environment, carbides of Group 5 (Niobium and Tantalum) and 6 (Chromium, Molybdenum, and Tungsten) were tested for hydrogen evolution activity and electrochemical stability in the temperature range between 80 and 170 °C.[130] Activities were found to be significantly higher for the Group 6 metal, with WC still exhibiting the best performance. With regards to stability, a passive behavior was noted for chromium, tantalum

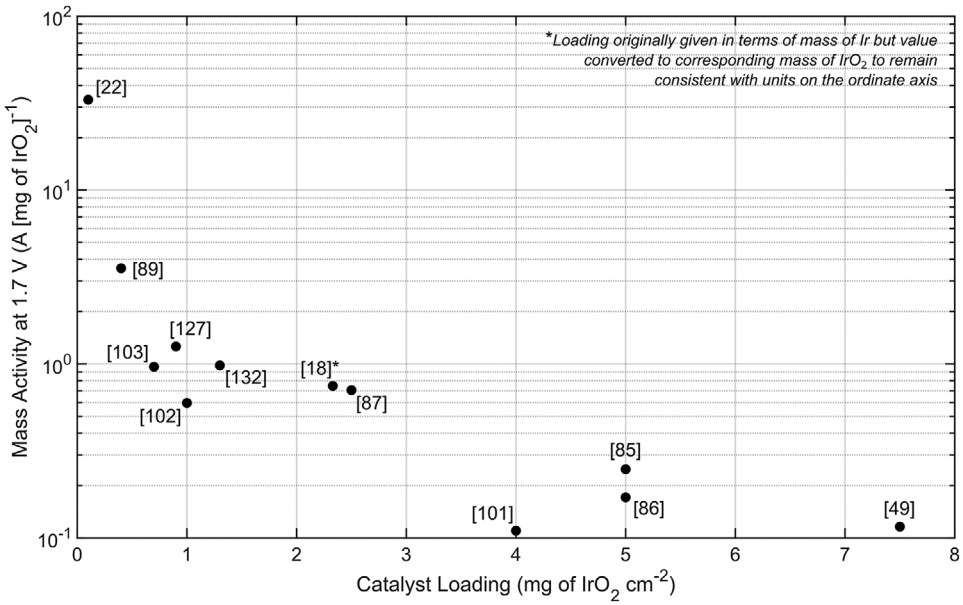

Figure 8. Mass activity as function of anode catalyst loading for ET studies.

and tungsten carbide films, while niobium and molybdenum carbides seemed to suffer from significant corrosion.

4.2.1. Optimizing Catalyst Loading

Higher catalyst loadings may not necessarily imply improved performance. An anode electrode with a loading of 2 mg cm^{-2} of IrO_2 prepared by spray coating was found to provide no substantial difference in performance to one with a loading of 0.1 mg cm^{-2} prepared by electro deposition.[22] The latter was equally capable of providing a comparable number of active sites available for the OER, albeit with a low noble metal loading. The study by Choe et al.[89] further assesses the impact of different catalyst loadings involving electrodeposited IrO_2. In this case, a certain loading threshold existed, above which the cell started to perform poorly. The authors attributed the change in performance (i.e. higher overpotentials) to possible cracking exposing the Ti surface and allowing it to oxidize. Moreover, surface roughening with prolonged catalyst deposition may promote mass transfer limitations.

Bearing in mind the limited availability of iridium and the energy capacities, which would need to be met,[19,131] its quantity in WE setups at some point needs to be considered in the cost equation. Utilizing mass activities (calculated by dividing the current density by the catalyst loading as done in the study by Choe et al.[89] and Lee at al.)[22] would allow a normalized benchmark with respect to a unit mass of loading, hence allowing better comparison of systems. **Figure 8** summarizes the mass activities for studies carried out at ET (when complete data was available).

4.2.2. Use of Support Structures

Catalyst utilization may be improved by dispersing the precious metal compound onto a catalyst support. The benefits of using support structures include i) an increase in specific surface area of the catalyst, hence providing an increased number of sites where the electrochemical reaction can occur, ii) improved homogeneity of electrocatalyst particles' dispersion, and iii) reduced probability of agglomeration.[127,132]

Support Structures Tested under Liquid Operation: TiO_2[127] and TaC[132] have been studied as potential anode catalyst supports for the more expensive IrO_2. It is interesting to note that the IrO_2 crystallite size remained relatively unchanged (i.e. within the experimental error) both when changing the support crystallite size and also when varying the support-catalyst weight proportion. Both studies reported improved performance over the unsupported catalyst and also acknowledged the usefulness of the support structure to limit the penetration of IrO_2 into the PTL rendering the catalyst inactive as it loses contact with the polymer electrolyte. On the other hand, both studies suggest a different view on the significance of electron conductivity in the resulting structure. Polonský et al.[132] dismiss its importance since the performance is in any case better than the unsupported alternative. However, Mazúr et al.[127] highlighted the need of maintaining an electronically conductive surface phase as support crystallite sizes below a certain threshold were found to be dispersed in isolated positions and hence not contributing to the overall conductivity, to the detriment of overall performance.

Support Structures Tested under Steam Operation: In the case of steam operation, a SiC-Si composite was studied as a support material for the IrO_2 catalyst.[133] Brunauer–Emmett–Teller (BET) measurements and cyclic voltammograms clearly indicated a greater specific surface area (and hence electrochemical activity) for the samples consisting of 80–90 wt% IrO_2 than for pure IrO_2. It should be noted however that the activity tended to decrease at higher temperatures (up to 150 °C), with the authors attributing such behavior to a loss of catalyst over time due to poor interaction with the support. Moreover, similar to the support structures discussed above, the conductivity was measured

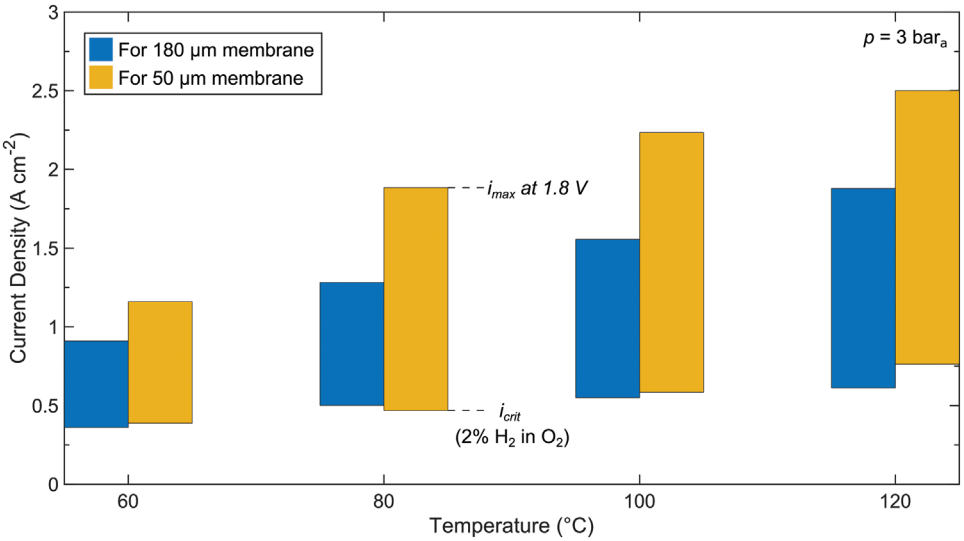

Figure 9. Current density ranges for safe operation and maximum efficiency as a function of temperature and membrane thickness (using data from Garbe et al.[18]).

to drop significantly with the introduction of the support composite. TaC has also been suggested as a potential support material for steam operation,[134] with this study focusing on the change of conductivity with time due to the formation of a surface oxide layer.

Another alternative studied in a steam environment involved tin oxides.[103] In particular, SnO_2 was doped with antimony (Sb) to also cater for improved electronic conductivity in the support. Indeed, the electronic conductivity of Sb-SnO_2 (5% Sb) was measured to increase by 400 times compared to that of pure SnO_2. On the downside, the stability of such structures has been questioned due to high anodic potentials resulting in the leaching of Sb.[135,136] Further to support structure adopted by Xu et al.,[103] addition of tin pyrophosphates (SnP) was expected to improve proton conductivity. While the addition of an ionomer may be expected to fulfil this function, it can also fill the void volume in such a way as to reduce the number of reachable catalyst active sites due to the pores becoming blocked, hence impairing performance.[137] In this regard, SnP_2O_7 as porous clusters allowed proton conductivity without impairing catalyst layer porosity. Cyclic voltammograms showed that, when compared to the unsupported IrO_2 catalyst, these different support configurations led to increasing the number of active sites in the following order: IrO_2, IrO_2/SnO_2, IrO_2/Sb-SnO_2 and IrO_2/SnP-(Sb-SnO_2), a result also evident in the lower voltages obtained in polarization experiments (when comparing all configurations operating in steam).

Also in view of coupling electric and proton conductivity in support structures, Xu et al.[104] proposed supports from tin doped indium oxides and proton conducting phosphates, structured with three-dimensionally ordered hexagonal arrays. Compared to the pure IrO_2 catalyst, the catalytic activity towards the OER improved by five times. When tested in a steam-based electrolyzer cell, the improved performance peaked at a temperature of 130 °C, after which an increase in ohmic resistance was observed, an effect attributed to the doping acid in the catalyst layer and membrane phase. It should be highlighted that indium tin oxides were also found to be susceptible to dissolution at high anodic potential.[135]

It follows from these studies that an optimal support structure must feature i) long-term stability, ii) provision of a high electrocatalytic surface area, and iii) good proton and electron conductivity.

4.2.3. Addition of a Recombination Catalyst

In PEMWE, hydrogen permeability and cross-over rates have been shown to increase with thinner membranes[18] and higher current densities,[138] temperatures,[139] ionomer cathode content,[140] and differential pressures between the membrane.[141] In **Figure 9**, the lower ends of each bar signify the current density threshold below which the H_2 in O_2 concentration increases by more than 2%, set as a safety limit to prevent an explosive mixture. The lower limit of current density at which the system can be safely operated, is hence driven to a higher value with ET.

Use of a recombination catalyst has been suggested to mitigate such hydrogen cross-over.[142,143] In this regard, Briguglio et al.[95] studied two different methods of including PtCo (as the recombination catalyst) in the MEA. One configuration involved the PtCo alloy catalyst integrated as a separate layer between the membrane and the IrRuOx anode catalyst (unmixed) while in the second configuration, the recombination catalyst was mixed in the same layer of the IrRuOx. When operated at 140 °C and pressures of 5.5 bar (at the anode) and 20 bar (at the cathode), the H_2 concentration in the oxygen stream was limited to ≈2% across the overall current density range (with data points starting from ≈0.2 A cm^{-2}). Only the mixed configuration was studied at the elevated temperature since this had shown reduced gas cross-over over the unmixed alternative at 55 and 90°C, albeit with a poorer electrochemical performance.

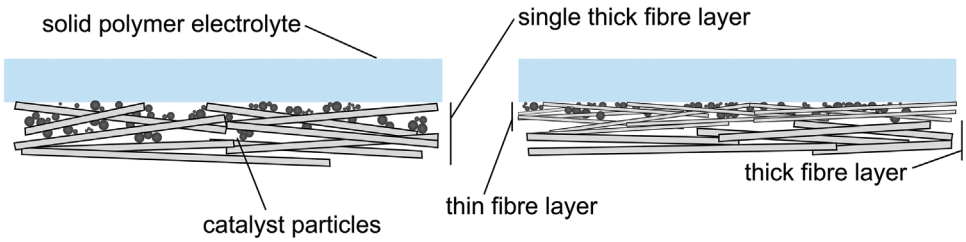

Figure 10. The study by Hansen et al.[102] showed how a catalyst-coated felt with thinner fibers close to the membrane (right image) improved catalyst utilisation.

4.3. Porous Transport Layer (PTL)

The porous transport layer is responsible for the mass transport of products and reactants of the electrolysis reaction while acting as an electrical conductor between the electrode and the bipolar plate. Its pores must hence be properly sized so as to allow fluid flow with minimal obstruction. Moreover, the PTL must also serve as mechanical support to the delicate membrane.[144]

At the cathode side, carbon-based materials (cloth/paper) are typically utilized, even at ET.[86,89,101] On the other hand, unlike in the case for PEM fuel cells which typically also use carbon materials on the anode side, titanium is generally adopted since the anodic potential is high enough to oxidize carbon material.[145] Titanium was used in differing forms involving meshes,[49,55,98,113] nets,[86,87] felts[92,95] and sintered powder structures.[18]

Li et al.[55] compare the effect of how the porous transport layer properties involving thickness, average pore diameter, and water contact angle affect the electrolysis cell performance at temperatures of 80 and 100 °C. As can be expected, smaller PTL thickness translates in better performance. However, in contrast to thickness, which plays a noticeable effect at both LT and ET, mean pore diameter played a much more pronounced effect at 100 °C. The average pore diameter was found to mainly influence the concentration overvoltage and an optimal pore diameter value exists, which provides a compromise between stronger capillary forces (improved with smaller pores) without obstructing gas removal (improved with larger pores). It should be highlighted that the study focused on a very particular operating condition coinciding with the boiling point of water (and no additional pressurization). The same study also showed the benefit of opting for hydrophilic surfaces with low contact angles. Moreover, the cathode side may also have a noticeable impact on performance.

An alternative to catalyst-coated membranes to produce the Membrane Electrode Assembly (MEA) involves spraying on the porous media. This method was adopted by Hansen et al.[102] to study two different felt arrangements on the anode side – one involving a single layer composed of fibers with a diameter of 12 µm and another involving a double-layer felt (introducing a type Microporous Layer, MPL) made up of 8 µm fibers and 12 µm fibers. The latter configuration was shown to display lower activation and ohmic overpotentials due to i) improved catalyst utilization arising from a more closed structure (i.e. denser) in the double-layer prohibiting deeper catalyst penetration and leaving it unutilized (**Figure 10**) and ii) the rougher topology promoting more contact points between the membrane and gas diffusion layer leading to a lower total resistance.

Accelerated degradation has been observed with the use of titanium bipolar plates and PTLs even for LT PEMWE[146] and additional protection layers to mitigate the harsh environment of the electrochemical reaction at the interface between PTL and the anode hence have been suggested.[147] It appears logical to use this kind of a protection for the ET case, where degradation is even more pronounced. In liquid water, Choe et al.[89] proposed electrodepositing IrO_2 (e-IrO_2) on the porous titanium mesh structure to serve as protection layer preventing oxidation of the inner titanium, besides providing for a catalyst layer for the oxygen evolution reaction. The improved degradation rate confirmed its suitability as a corrosion-protective film. Xu et al.[113] also opted for a gold-coated PTL.

In the case of steam operation, tantalum-coated stainless steel felt has been utilized as a replacement to titanium as a more corrosion resistant material in a phosphoric acid environment.[101,102,104] Tantalum has been shown to display and maintain low interfacial contact resistances at the PTL/ bipolar plate interface.[148]

In summary, very little work has been done to investigate optimum PTL structures for different operation scenarios. Particularly finding optimum PTL structures at different temperatures and operation conditions (e.g. liquid vs. steam) remains an open field.

4.4. Test Stand and Cell Setup

Higher temperatures present an even more challenging environment–this section therefore highlights a number of points related to the test station and cell setups, which have been considered to cater for the operating conditions in question.

4.4.1. Operating Conditions

Provision of a stable and sufficient water flowrate is indispensable to mitigate mass transfer limitations giving rise to concentration overpotentials, with water utilization, defined as the proportion of electrolyzed water to fed water, typically taken as 0.5%.[88] Setups for ET PEMWE have either input water to the cell from both anode and cathode sides[98,113] or solely from the anode compartment.[22,55,85–89,95,127,132,149]

While the absence of recirculation on the cathode side was not observed to have an effect on the i-V curve at LT in the case of Ito et al.,[150] other studies reported water accumulations in the cathode compartment giving rise to higher voltages.[151,152] Improved performances were in fact noted with nitrogen purging,

which prevented water slug entrapments in the flow channel[153] or blockages closer to the membrane region.[88,152] Moreover, an optimal flowrate exists, which removes water to prevent blockage while not being itself a source for membrane dehydration.[153] It would indeed be interesting to observe the effect of these different configurations at ET, especially when such conditions are more likely to induce membrane dry-out with lack of water.[85,86,154]

The improved performance of ET comes at the expense of higher heating requirements. This has been provided for with different methods such as with the use of an in-line heating[18] or by placing the cell in an oven.[49] Another method simply involved allowing the water to enter the cell at room temperature and only acclimatize to the operating temperature within the heated cell.[55] This was only possible due to the low flowrates involved. In the case of steam, an even higher heating input is required to provide for the latent heat of vaporization for the change of state. This was achieved by a custom-built evaporator device consisting of many small-sized spheres so that heating is performed on a large surface area.[111]

In the case of liquid water operation, the system is pressurized to increase the saturation temperature of water, typically performed with back pressure valves.[18]

Ion exchangers may be implemented in a re-circulating system so as to remove any impurities, which may have leached into the water and to potentially affect both membrane conductivity and the durability of the electrode.[155] Alternatively, PTFE tubing may be used which would mitigate any ion leaching from the test station hardware. Nonetheless, temperature limits of PTFE tubing tend to substantially decrease with increasing pressure requirements (from as low as 5 bar).

4.4.2. Bipolar Plate Materials

In general, titanium was the material of choice for the bipolar plates on the anode side[55,88,92,115,127] while graphite or carbon was employed on the cathode side.[22,55,88,89] The interfacial contact resistance has been however shown to increase with time.[156] In this regard, coatings of gold[92,115,127] or tantalum[102,132] have been applied on titanium or stainless steel for improved corrosion resistance.

Nikiforov et al.[106] studied different types of commercially available stainless steels, Ni-based alloys, titanium, and tantalum as a possible material for bipolar plates in a phosphoric-acid based environment up to a temperature of 120 °C. Tantalum showed the best corrosion resistance while the typically-adopted titanium exhibited the poorest resistance.

4.4.3. Flow Field Patterns

Li et al.[149] studied the effect of flow patterns on electrolysis performance–namely, serpentine, cascade, and parallel patterns. On the cathode side, the serpentine and cascade patterns displayed a similar performance, and better than the parallel alternative. The authors attribute this result to a pressure difference, which is created between the channels causing an under-rib convective flow through the PTL and hence more water being made available to the membrane. The differential pressure between neighboring channels in the parallel pattern is too low to create such an effect. Interestingly, a different flow pattern displayed the best performance on the anode side, with the cascade pattern providing the lowest voltages and the serpentine pattern exhibiting the highest. In this case, analysis of HFR characteristics and Tafel plots indicated that the difference stemmed from liquid water shortage, with lower flow velocities promoting more favorable water saturation properties in the PTL. In the anode case, the effect of pressure difference (described above for the cathode side) was considered to only exert a minor effect due to differences in PTL materials–in contrast to the hydrophobic carbon cathode surface, the capillary forces in the hydrophilic titanium surface (on the anode side) exert a much greater role in fluid transport.

5. Performance of ET PEMWE

Section 4 has summarized the key conclusions of recent developments in the MEA and cell setups carried out at ET. This section is intended to look at the system performance from a broader perspective with respect to input power, operating phase and results from mathematical modeling.

5.1. Input Power Requirements

In general, studies confirm the progressively reduced voltage requirements with ET,[85,98,113,149] as predicted by the Nernst equation. Together with presenting the key characteristics of studies involving full-cell tests performed at ET, **Table 2** summarizes the current density obtained at the thermoneutral voltage ($i_{TN,}$ 1.48 V) and 1.7 V (as a more relevant cell voltage at the industrial level). However, it should be highlighted that any comparison should be done with care since the electrical resistance varies with different cell setups. Moreover, a higher catalyst loading may also affect performance, albeit at increased costs. In this regard, as performed in the study by Choe et al.,[89] the mass activities were calculated for each study and have been plotted in Figure 8.

A direct comparison in performance solely based on operating phase (steam or liquid water) is hindered by the fact that different membranes have been employed.[88] It is hence worth looking at the different classes of membranes utilized when comparing the two operating phases. This builds on what has been discussed in Section 4.1 and confirms the need of further research on membrane material suitability at ET.

Employing a PFSA-based membrane has consistently shown mass transport limitations with increasing current density under steam conditions.[85,86,88] Lee et al.[22] distinguish the different overpotentials at 120 °C under different pressures. Only in the case of atmospheric pressure (and steam) there is evidence of a concentration overvoltage at a current density as low as 0.5 $A{\cdot}cm^{-2}$. An adequate concentration gradient is then restored with pressurization, whereby the saturation temperature of water is increased, allowing the cell to be flooded with liquid water (**Figure 11a**). This indeed is to be expected given that PFSAs generally work through conducting mechanisms heavily dependent on the water content.[53] This property is lost with steam as the membrane equilibrates to a lower λ and loses conductivity.

Table 2. Key characteristics and cell performance of PEMWE at ET.

Study	Temperature [°C]	Pressure [bar]	Studied Phase(s)	Membrane	Catalyst (Loading)		i_{TN} [mA cm^{-2}][a)]	$i_{1.7\,V}$ [mA cm^{-2}][a)]
					Anode [mg cm^{-2}]	Cathode [mg cm^{-2}]		
[85]	80–120	1, 3	Both liquid and steam	Composite SiO_2-Nafion	IrO_2 (5)	Pt (0.8)	250	1240
[86]	80–120	1, 3 (anode only)	Both liquid and steam	Composite TiO_2-Nafion	IrO_2 (5)	Pt (0.8)	364	856
[115]	80, 120	1, 3	Liquid	PSU-reinforced and non-reinforced Aquivion	$Ir_{0.7}Ru_{0.3}O_x$ (1.5)	Pt (0.5)	717	Not Available[b)]
[87]	80, 100	1	Liquid	Composite Nafion/sulfated zirconia	IrO_2 (2.5)	Pt (0.5)	416	1768
[88]	80–130	1–5	Both liquid and steam	Nafion 117	IrO_2 (1.5)	Pt (0.5)	Cell voltage given as a function of temperature but only at a fixed current density of 1 A cm^{-2}	
[113]	80–130	1.5–5	Liquid	Composite PFSA-silica (commercial)	$Ru_{0.7}Ir_{0.3}O_2$ (2.5)	Pt (0.6)	837	Not Available[b)]
[89]	120	2.5	Liquid	Nafion 212	IrO_2 (0.01–2.69)	Pt (0.4)	445	1421
[22]	120	1–2.5	Both liquid and steam	Nafion 212	IrO_2 (0.1;2)	Pt (0.4)	661	3307
[55]	80, 100	1	Liquid (at Boiling Point)	Nafion 117	IrO_2 (1.5)	Pt (0.5)	587	Not Available[b)]
[101]	130	1	Steam	PA-doped Nafion or PA-doped PBI or PA-doped Nafion/PBI blends	IrO_2 (4)	Pt (0.7)	116	439
[102]	130	1	Steam	PA-doped Aquivion	IrO_2 (1)	Pt (0.8)	130	597
[127]	90–130	3	Liquid	Nafion 117	IrO_2 (0.9)	Pt (0.5)	176	1134
[132]	90–130	3	Liquid	Nafion 117	IrO_2 (1.3)	Pt (0.5)	217	1275
[98]	100–120	3	Liquid	Aquivion E87-123; Composite Aquivion E87-123-ZrP; sPBI-OO	IrO_2 (2)	Pt (2)	331	Not Available[b)]
[49]	80–150	1	Liquid/Steam	Nafion 115	IrO_2 (7.5)	Pt (0.3)	77	868
[100][c)]	80–150	1	Liquid/Steam	CSPPSU	IrO_2 (not available)	Pt (0.3)	12	238
[109]	80, 100	1	Liquid (at Boiling Point)	Undoped Nafion and composite Nafion/sulfated titania	$Ir_{0.7}Ru_{0.3}O_x$ (1.5)	Pt (0.5)	572	1742
[18]	60, 80, 100, 120	3	Liquid	Nafion 117 and Nafion 212	Ir (2)	Pt (0.4)	338	1745
[104]	80, 110, 130, 150, 170	1	Steam	PA-doped Aquivion	IrO_2 (0.7)	Pt (0.7)	273	Not Available[b)]
[103]	80, 130	1	Steam	PA-doped Aquivion	IrO_2 (0.7)	Pt (0.7)	135[d)]	674[d)]
[149]	80, 100, 120	1, 3	Liquid	Nafion 117	IrO_2 (1.5)	Pt (0.5)	498	Not Available[b)]
[111]	120	3	Liquid	Recast Nafion 5 wt% BPO_4	IrO_2 (3.31)	Pt (0.8)	116	631
[95]	140	5.5 (anode) 1;5;10;20 (cathode)	Liquid	Aquivion	IrRuOx (1.5)	Pt (0.1)	311	3492

[a)] WebPlotDigitizer was used for data extraction;[157] [b)] Data points stop before a voltage of 1.7 V is reached – even though in some studies, the last data point is just shy of 1.7 V, no extrapolation was performed in these cases; [c)] Experimental details given in previous publication by the same authors;[49] [d)] Results originally given in mA·[mg(IrO_2)]$^{-1}$, but respective catalyst loading was used for conversion to mA·cm^{-2}; General note: data extracted only for best performing polarization curves

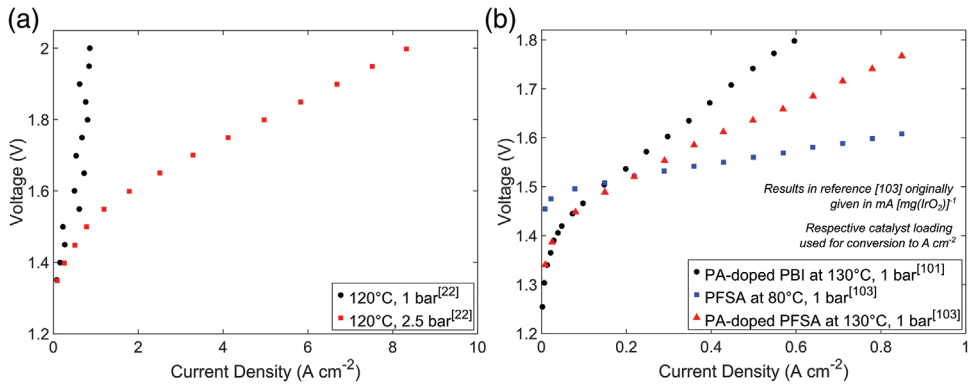

Figure 11. Superimposing polarization curves at different operating conditions and utilizing different membrane types as indicated in the respective legends: a) PFSA based and b) PBI based.

PA-doped PBI membranes were hence utilized as an alternative for steam conditions. As observed from the lower end of the current density range in Figure 11b, ET under steam conditions displayed lower voltages (cf. Section 2.1) despite the slowed catalyst activity in a phosphate environment.[128] However, sub-optimal humidification resulted in increasing ohmic overpotentials with steam, evidenced by the steeper gradients (compared to liquid water operation at 80 °C). Indeed, the lower water content causes a drop in the conductivity of phosphoric acid, causing the latter to start polymerizing and the charge carrier H_3O^+ becoming scarce.[53] PA was also doped to PFSA membranes as shown by the additional curve in Figure 11b. Successful operation of PA-doped PFSAs is attributed to the higher water activity in WE mode–contrary to operation in FC systems.[158]

In general, more studies are dedicated to liquid operation rather than steam at ET conditions. **Figure 12** collectively compares the performance of all ET studies based on whether these were carried out in steam or in liquid. As concluded by Jensen et al.,[53] lower voltages and higher current densities seem to currently favor operation with liquid water (signified by the yellow shaded area).

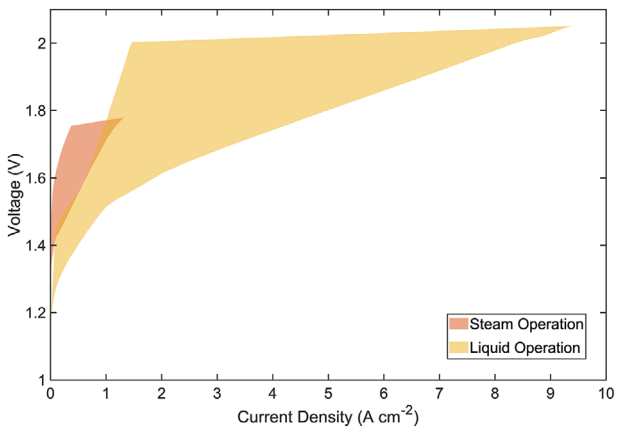

Figure 12. Shaded regions capture the best performances obtained for steam operation (up to a temperature of 170 °C)[49,100–104] and liquid operation (studied in the temperature range of 100–140 °C and under a pressure up to 5.5 bar_{abs} on the anode side).[18,22,55,85–87,89,95,98,113,115,127,132,149]

5.2. Mathematical Modeling and Efficiency

The results presented so far have been mainly based on experiments, an approach that is very time-consuming, expensive, and may not necessarily resolve in detail what is happening within the cell.[159] In this regard, mathematical modeling can also provide insight of performance, assessing varying aspects such as the microfluidics within the cell, control strategies in operating a plant and the expected energy and exergy efficiencies. The following further details modeling efforts specifically for ET PEMWE.

Zhao et al.[160] presented a 2D multiphysics model of a steam-based system at 130 °C to assess the influence of applied voltage, anode water mass fraction, and inlet steam velocities on energy efficiency. The applied voltage gives rise to a varying temperature and current density along the main flow stream, while increasing the mass fraction of anode water would improve reactant concentration and hence allow higher current densities to be achieved. Increased gas velocities not only improve provision of the reacting species but also take away heat from the electrolyzer and stabilize cell temperatures. All studied parameters were found to affect the overall energy efficiency and by specifying the possible operating range for each of the studied parameters, the model also provided the optimal parameter values, which promise the highest efficiency.

The model by Kai et al.[161] takes into account the gas/liquid behavior near the catalyst layer and the variation of gas saturation with ET by including the effect of bubble formation on the exchange current density of the activation overpotential. Validated against experimental data, the model shows how a decreasing activation overpotential is largely responsible for the reduction in voltage requirements with higher temperatures. This improvement however is hampered as the gas saturation increases when the saturation temperature is approached. The model clearly shows the benefit of increasing the pressure to delay the activation overpotential increase. The study also suggests pressure limits as a function of temperature and current density to maintain the gas saturation below a threshold, which would impair performance.

Simulation also involved the use of a Computational Fluid Dynamics (CFD) based numerical model capable of solving for mass, species, energy, and momentum conservation.[162] The model managed to simulate the general trend of lower voltages observed in polarization curves with ET. Moreover, specific to CFD analyses, it also provided color plots of the variation of temperature and species' concentrations at the membrane catalyst interface. CFD was also used as the basis to calculate energy and exergy efficiencies as a function of current density.[163,164] Considering a current density of 1 A cm^{-2}, an efficiency improvement of ≈2.5% points was obtained when increasing the temperature from 80 to 120 °C. (The energy and exergy efficiency were found to be very close in all cases, indicating a low exergy degradation in the system). This analysis was extended to perform an exergo-economic analysis, whereby the monetary saving could be computed as a result of the efficiency improvement. Another application for CFD involved analyzing different flow channel geometries for steam conditions based on thermal distribution, hydrogen production and pressure drop.[165]

On the premise that higher temperature differences allow improved heat management, a system was proposed, which utilizes the heat losses from the stack irreversibility to heat the dosing water, make up for the losses in the pipework and stack and if surplus is available, utilize it for a secondary application such as district heating.[27] Energy and exergy efficiency were in this case also utilized as the performance metrics. The model showed that the stack operates in autothermic mode over a considerable range of current density and the heating inputs to the stack and feed water become progressively unnecessary. The exergy efficiency for the ET operation was calculated to surpass that for LT operation, with the maximum improvement reaching 3.8%.

While acknowledging that the use of hydrogen can be a means to deal with the intermittency of renewables, hydrogen production systems must be capable of handling possible fluctuations and high overshoots, which could result in poor durability and performance.[159] For instance, Zhao et al.[166] studied the dynamic response of ET PEMWE in the start-stop and adjustment phase by assessing the effect of different voltage regulation schemes (step, multistep or diagonal) on different aspects of WE operation such as electrochemical response (in terms of reactants' starvation) and temperature response (in terms of excessive gradients). The results were then used to come up with the safest and fastest dynamic process adjustment scheme.

A follow-up study also looked at the effect of using different data-driven methods to handle the fluctuations in input power.[159] For instance, a neural network predictive control strategy was found to reduce the power overshoot by ≈92% when compared to a fuzzy control strategy. The study also includes the effect on the dynamic response on produced hydrogen, temperature, and efficiency changes.

Zhao et al.[167] also studied the effect of optimizing the anode gas inlet flow rate during intermittent operation. In this case, the implemented model involved steam operation and hydrogen recirculation on the cathode side to reduce thermal energy demand. Using what was termed as the cooperative model predictive strategy, the model determines the anode gas inlet flow rate required for the particular power consumption such that the maximum efficiency point is continually tracked. The model also plays a role in limiting change rate of current density. Besides mitigating reactant starvation, this approach was found to improve efficiency during the dynamic process by ≈1.2% (compared to a strategy involving a fixed supply of steam).

5.3. Stability and Degradation

The performances in Figure 12 would also need to be maintained throughout the electrolyzer's system lifetime. However, the strongly acidic and oxidative environment in PEMWE presents a very challenging framework, which may give rise to multiple degradation mechanisms for the various components making up the cell.[17] Nonetheless, LT operation has been shown to run very reliably with no detectable voltage loss over a life span running in the range of thousands of hours.[168]

A number of studies looked at the behavior of ET cells in terms of the current drop (at a fixed voltage) or voltage rise (at a fixed current density) with time. **Table 3** summarizes the details of the studies, which have considered degradation at ET. The loss of performance is observed by a drop in current density (from the negative values of the first three entries) or higher voltages (deduced from the positive values in the last three entries).

Membrane dehydration at ET has been considered to play a significant role in the poor stability performance observed with Nafion.[49,85] In an effort to opt for non-fluorinated electrolyte membranes, Kim and Ohira[100] suggest the use of cross-linked sulfonated polyphenylsulfone (CSPPSU). The stability of this material under wet conditions was investigated in water at 85 °C for 3600 h (150 days) and in an autoclave at 150 °C for 2184 h (91 days). No significant differences were observed when testing for the IEC and conductivity before and after membrane treatment. Moreover, no observable changes were observed from SAXS measurements when measuring the change with an increase in the temperature from room temperature to 180 °C and back. However, when carrying out full-cell tests over an extended period of time (using CSPPSU), EIS results and the subsequent cell disassembly led to the conclusion of the need to improve the interface between the membrane and the electrode. For tests carried out with PA-doped membranes, the lack of stability was mainly observed in the first 100 h, possibly due to loss of doping acid in the catalyst layers and membrane upon starting to feed with steam.[103,104] From another perspective, Choe et al.[89] showed that electrodeposition (of IrO_2 on a Ti substrate) resulted in a significantly enhanced durability compared to electrodes manufactured using the spray-coating method.

It is, however, the work by Garbe et al.[169] which by far gives a very comprehensive study on degradation effects at ET operation. The performance of two cells was compared–one operating at 60 °C (*Cell 1*) and another at 100 °C (*Cell 2*), both at an absolute pressure of 3 bar. Nafion 117 was used as the membrane and the iridium and platinum catalyst loadings respectively consisted of 2.1 and 0.4 mg cm^{-2}. Multiple in situ and ex situ techniques were employed so as to obtain a holistic picture of the predominant degradation mechanisms. Loss in performance over time is accentuated with higher operation temperatures.[170,171] In fact, at a constant current density of 2 A cm^{-2}, voltage loss rates of 29 and 126 μV h^{-1} were respectively reported for 60 and 100 °C over

Table 3. Degradation experiments from literature data involving ET operation.

Study	Temp. [°C]	Pressure [bar_{abs}]	Operating Condition	Operating Time [hours]	Membrane	Catalyst (Loading)		PTL	GDL	Degradation Rate
						Anode [mg cm^{-2}]	Cathode [mg cm^{-2}]			
[85][a)]	120	3	1.5 V	300	Composite SiO_2-Nafion	IrO_2 (5)	Pt (0.8)	Ti backing	carbon cloth	−0.39 mA cm^{-2} h^{-1}
[49][a),b)]	120	1	1.7 V	8	Nafion 115	IrO_2 (7.5)	Pt (0.3)	Ti powder porous sheets (500 µm)	carbon fiber paper (235 µm)	−18.9 mA cm^{-2} h^{-1}
[100]	120	1	1.7 V	8	CSPPSU	IrO_2 (n.a.)[c)]	Pt (0.3)	Ti powder sheet[d)]	carbon fiber paper (235 µm)	Current density drops[e)] close to 0 mA cm^{-2}
[89]	120	2.5	1.72 V	300 (e-dep) or 150 (spray)	Nafion 212	IrO_2 (0.4)	Pt (0.4)	Ti-based	carbon fiber paper (325 µm)	−1.5 mA cm^{-2} h^{-1}−3.93 mA cm^{-2} h^{-1}
[104][a)]	130	1	0.35 A cm^{-2}	~ 1200	PA-doped Aquivion	IrO_2 (0.7)	Pt (0.7)	Ta-coated stainless steel felt	Non-woven carbon cloth	+ 0.09 mV h^{-1}
[103][a)]	130	1	0.4 A cm^{-2}	760	PA-doped Aquivion	IrO_2 (0.7)	Pt (0.7)	Ta-coated stainless steel felt	Non-woven carbon cloth	+ 0.114 mV h^{-1}
[169]	100	3	2 A cm^{-2}	300	Nafion 117	Ir (2.1 ± 0.1)	Pt (0.4 ± 0.05)	Sintered Ti (1 mm)	Carbon sheet (1.5 mm)	+ 0.126 mV h^{-1}

[a)] WebPlotDigitizer[157] was used for data extraction; [b)] Degradation rate calculated as the average over three runs; [c)] Information not available in study; [d)] Sample 1 used in previous publication by Kim and Ohira[49] was chosen to be used in follow-up study;[100] [e)] Issues in the assembly of the CSPPSU membrane and the electrode observed to possibly be the reason for the poor performance, rather than the membrane stability itself.

a testing duration of 300 h.[169] Such rates would mean that the initial performance gains for *Cell 2* obtained by the higher operation temperature would be consumed after a projected operation time of 3 500 h. From a breakdown of overpotentials before and after the experiment, kinetic and ohmic losses were mainly blamed for the higher voltages. Based on data from cyclic voltammograms, the number of active sites on the anode catalyst layer reduced by as much as 49% at ET. Moreover, a significant decrease was observed in the layer thickness.[169] Catalyst detachment due to a higher volumetric gas production and dissolution arising from the loss of the titanium-based support may possibly explain the loss of catalyst. With regards to the membrane, measurements of the Fluoride Release Rate (FRR) on PFSA-based materials have shown chemical ionomer decomposition even by just increasing temperatures up to 80–90 °C.[170,172–175] The FRR is also documented to approximately increase by two orders of magnitude as the temperature rises from 55 to 150 °C.[171] Operating at 100 °C and based on a 10% threshold loss of the initial fluoride inventory, the cell was forecasted to operate for not more than 3 700 h. In the case of the PTL and flow fields, the passivation of titanium,[176] which is further accelerated at ET,[59] results in higher ohmic overpotentials.[169] This calls for the need of more resistant materials such as W or Nb or the application of protective coatings.[89,177]

Figure 13, reproduced from Garbe et al.,[169] summarizes the multiple degradation causes and effects due to ET for the various cell components–each cause ultimately negatively impacting the system with regard to performance, cost and safety.

It is interesting to note that except in the case of Garbe et al.,[169] all stability-related studies resort to a low voltage or current density as the test condition. Acknowledging that the search of suitable membranes for ET PEMWE is still at its infancy, a wider test range would also provide valuable information on the stability behavior with respect to different loads.

6. Conclusion and Final Remarks

This review has summarized the discussions and results obtained to date for PEMWE at ET by looking in detail at studies involving full-cell testing. This background facilitated the identification of the key issues at a cell and system level. ET PEMWE are indeed expected to offer a number of key advantages, namely–a reduction of the specific energy demand, a reduction of catalyst loading or the employment of less noble electro catalysts and better waste utilization when the electrolyzer is operated in exothermal mode. Nonetheless, more research efforts are indeed required to have a clearer picture of the feasibility of PEMWE at elevated temperature.

The use Nafion at ET is hampered by the accelerated drop in conductivity with time and accelerated rates of chemical decomposition. On the other hand, PA-doped PBI membranes or other alternative membranes have not yet matched the electrochemical performance obtained with PFSAs. There is hence still a need for the development of membrane materials with improved thermal, mechanical, and chemical stabilities at ET. This need also extends to the choice of ionomer in the catalyst layer. Changes to

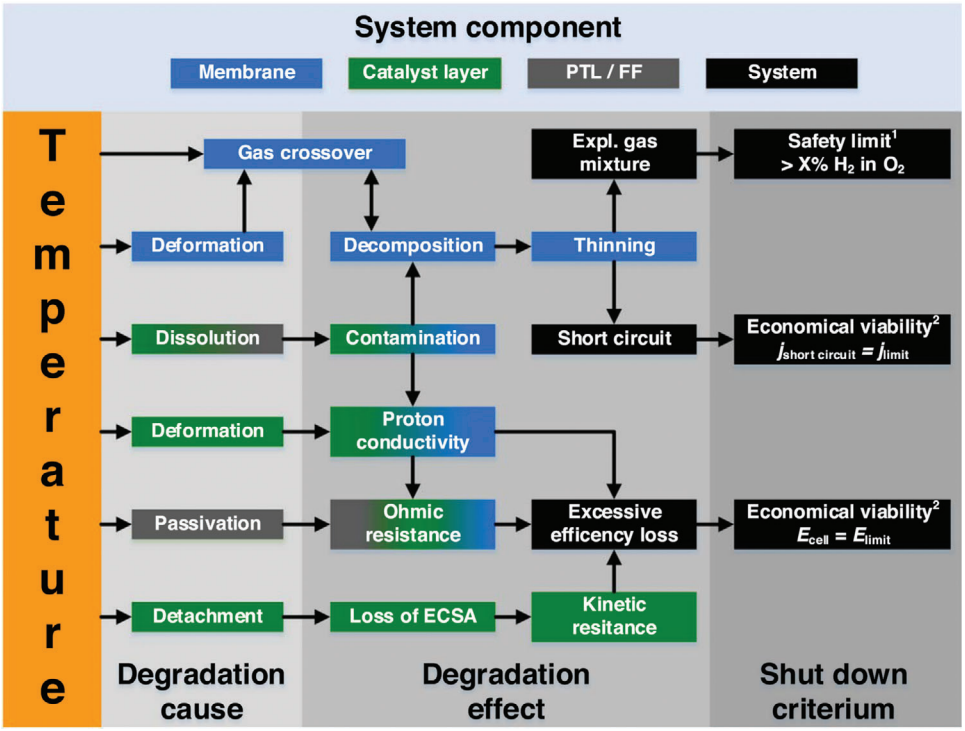

Figure 13. The causes and effects of ET for the different components used in PEMWE eventually affect performance, cost, and safety as given by the three shutdown criteria at the right end. Reproduced with permission.[169] Copyright 2021, The Electrochemical Society and IOP Publishing. All rights reserved.

the volumetric gas production rates at ET, or simply the use of steam, may require the re-evaluation of the optimization of PTL properties (such as porosity, thickness, texture, and pore diameter). Moreover, the harsher operating conditions also call for a re-assessment of optimal materials, an issue that strongly also applies to the bipolar plates. On the other hand, operating at ET conditions may bring about the possibility for finding improved catalysts whose activity, electrolyte compatibility, and stability is enhanced. Another benefit involves the higher-grade waste energy due to increased temperature differences. Its optimal use by integration to techniques such as combined cooling, heating, and power or ORCs for instance, would definitely need to be studied. Given the novelty of the technique, studies involving ET have so far focused on the cell, but due consideration would also be expected to be needed at a system level for the respective ancillaries. Further experimental results and mathematical modeling would in turn allow techno-economic analyses to ultimately assess whether efficiency gains would translate to monetary savings, and to what extent.

PEMWE at ET does promise a number of advantages, and the numerous challenges and unanswered questions should hence not be a reason to dismiss this technology, but rather serve as a beacon to the efforts in assessing its feasibility.

Acknowledgements

This work was financially supported by the Federal Ministry of Education and Research in Germany within the project HOPLYT (grant number: 03SF0666A) and Independent Research Fund Denmark (BICON,0217-00074B).

Open access funding enabled and organized by Projekt DEAL.

Conflict of Interest

The authors declare no conflict of interest.

Keywords

elevated temperatures, PEM water electrolysis

Received: February 23, 2023
Revised: November 30, 2023
Published online: December 18, 2023

[1] *World Energy Transitions Outlook: 1.5°C Pathway. International Renewable Energy Agency*, IRENA, Abu Dhabi, UAE **2021**.
[2] H. Yang, M. Driess, P W. Menezes, *Adv. Energy Mater.* **2021**, *11*, 2102074.
[3] C. V. Pham, D. Escalera-López, K. Mayrhofer, S. Cherevko, S. Thiele, *Adv. Energy Mater.* **2021**, *11*, 2101998.
[4] M. Chatenet, B G. Pollet, D R. Dekel, F. Dionigi, J. Deseure, P. Millet, R D. Braatz, M Z. Bazant, M. Eikerling, I. Staffell, P. Balcombe, Y. Shao-Horn, H. Schäfer, *Chem. Soc. Rev.* **2022**, *51*, 4583.
[5] I. Vincent, D. Bessarabov, *Renew. Sustainable Energy Rev.* **2018**, *81*, 1690.
[6] S. A. Grigoriev, V. N. Fateev, D. G. Bessarabov, P. Millet, *Int. J. Hydrogen Energy* **2020**, *45*, 26036.

[7] D. Henkensmeier, M. Najibah, C. Harms, J. Žitka, J. Hnát, K. Bouzek, *J. Electrochem. Energy Conv. Storage* **2021**, *18*, 024001.
[8] D. Hua, J. Huang, E. Fabbri, M. Rafique, B. Song, *ChemElectroChem* **2023**, *10*, 202200999.
[9] H. A. Miller, K. Bouzek, J. Hnat, S. Loos, C. I. Bernäcker, T. Weißgärber, L. Röntzsch, J. Meier-Haack, *Sustainable Energy Fuels* **2020**, *4*, 2114.
[10] J. Yang, M Je Jang, X. Zeng, Y. S. Park, J. Lee, S. M. Choi, Y. Yin, *Electrochem. Commun.* **2021**, *131*, 107118.
[11] T. Wang, X. Cao, L. Jiao, *Carbon Neutral.* **2022**, *1*, 21.
[12] O. Schmidt, A. Gambhir, I. Staffell, A. Hawkes, J. Nelson, S. Few, *Int. J. Hydrogen Energy* **2017**, *42*, 30470.
[13] P. Millet in *Compendium of Hydrogen Energy*, Vol. *1* (Eds: V. Subramani, A. Basile, T. Nejat Veziroğlu), Elsevier, Amsterdam, Netherlands **2015**, Ch. 9.
[14] A. Brisse, J. Schefold, A. Leon in *Electrochemical Power Sources: Fundamentals, Systems, and Applications – Hydrogen Production by Water Electrolysis* (Eds: T. Smolinka, J. Garche), Elsevier, Amsterdam, Netherlands **2021**, Ch. 7.
[15] A. Pandiyan, A. Uthayakumar, R. Subrayan, S. W. Cha, S. B. Krishna Moorthy, *Nanomater. Energy* **2019**, *8*, 2.
[16] W. Zhang, M. Liu, X. Gu, Y. Shi, Z. Deng, N. Cai, *Chem. Rev.* **2023**, *123*, 7119.
[17] Q. Feng, X.-Z. Yuan, G. Liu, B. Wei, Z. Zhang, H. Li, H. Wang, *J. Power Sources* **2017**, *366*, 33.
[18] S. Garbe, J. Futter, T J. Schmidt, L. Gubler, *Electrochim. Acta* **2021**, *377*, 138046.
[19] U. Babic, M. Suermann, F N. Büchi, L. Gubler, T J. Schmidt, *J. Electrochem. Soc.* **2017**, *164*, F387.
[20] U. Babic, E. Nilsson, A. Pătru, T J. Schmidt, L. Gubler, *J. Electrochem. Soc.* **2019**, *166*, F214.
[21] M. Bernt, A. Siebel, H A. Gasteiger, *J. Electrochem. Soc.* **2018**, *165*, F305.
[22] B.-S. Lee, H.-Y. Park, I. Choi, M. K. Cho, H.-J. Kim, S. J. Yoo, D. Henkensmeier, J. Y. Kim, S. W. Nam, S. Park, K.-Y. Lee, J. H. Jang, *J. Power Sources* **2016**, *309*, 127.
[23] C. Rozain, E. Mayousse, N. Guillet, P. Millet, *Appl. Catal., B* **2016**, *182*, 153.
[24] T R. Cook, D K. Dogutan, S Y. Reece, Y. Surendranath, T S. Teets, D G. Nocera, *Chem. Rev.* **2010**, *110*, 6474.
[25] W. Sheng, M. Myint, J. G. Chen, Y. Yan, *Energy Environ. Sci.* **2013**, *6*, 1509.
[26] S. Trasatti, *J. Electroanal. Chem. Interfacial Electrochem.* **1972**, *39*, 163.
[27] M. Bonanno, K. Müller, B. Bensmann, R. Hanke-Rauschenbach, R. Peach, S. Thiele, *J. Electrochem. Soc.* **2021**, *168*, 094504.
[28] W. J. Tiktak, *Master Thesis*, Delft University of Technology, Netherlands **2019**.
[29] H. Q. Nguyen, B. Shabani, *Energy Convers. Manag.* **2020**, *204*, 112328.
[30] S. Rashidi, N. Karimi, B. Sunden, K. C. Kim, A. G. Olabi, O. Mahian, *Prog. Energy Combust. Sci.* **2022**, *88*, 100966.
[31] J. Siecker, K. Kusakana, B. P. Numbi, *Int. J. Hydrogen Energy* **2022**, *47*, 32692.
[32] N. Briguglio, M. Ferraro, G. Brunaccini, V. Antonucci, *Int. J. Hydrogen Energy* **2011**, *36*, 8023.
[33] M. J. Moran, H. N. Shapiro, D. D. Boettner, M. B. Bailey, *Fundamentals of Engineering Thermodynamics*, Wiley, New Jersey, USA **2014**.
[34] B. Orr, A. Akbarzadeh, M. Mochizuki, R. Singh, *Int. J. Hydrogen Energy* **2016**, *101*, 490.
[35] H. Kim, S. Choe, H. Park, J. H. Jang, S. H. Ahn, S. Kim, *Nanoscale* **2017**, *48*, 19045.
[36] F. Hegge, F. Lombeck, E. Cruz Ortiz, L. Bohn, M. von Holst, M. Kroschel, J. Hübner, M. Breitwieser, P. Strasser, S. Vierrath, *ACS Appl. Energy Mater.* **2020**, *3*, 8276.
[37] J. P. Hughes, J. Clipsham, H. Chavushoglu, S. J. Rowley-Neale, C. E. Banks, *Renew. Sustain. Energy Rev.* **2021**, *139*, 110709.
[38] T. Lim, S. Kim, *Chem. Eng. J.* **2022**, *433*, 133681.
[39] A. Martin, P. Trinke, C. van Pham, M. Bühler, M. Bierling, P. K. R. Holzapfel, B. Bensmann, S. Thiele, R. Hanke-Rauschenbach, *J. Electrochem. Soc.* **2021**, *168*, 114513.
[40] A. Rajora, J. W. Haverkort, *J. Electrochem. Soc.* **2021**, *168*, 034506.
[41] A. Weiß, A. Siebel, M. Bernt, T.-H. Shen, V. Tileli, H. A. Gasteiger, *J. Electrochem. Soc.* **2019**, *166*, F487.
[42] M. Suermann, *Doctoral Thesis*, ETH Zurich, USA, **2017**.
[43] J. Mo, *Doctoral Thesis*, The University of Tennessee, Knoxville, USA, **2016**.
[44] S. Stiber, N. Sata, T. Morawietz, S. A. Ansar, T. Jahnke, J. K. Lee, A. Bazylak, A. Fallisch, A. S. Gago, K. A. Friedrich, *Energy Environ. Sci.* **2022**, *15*, 109.
[45] J. Parra-Restrepo, R. Bligny, J. Dillet, S. Didierjean, D. Stemmelen, C. Moyne, A. Degiovanni, G. Maranzana, *Int. J. Hydrogen Energy* **2020**, *45*, 8094.
[46] T. Schuler, R. De Bruycker, T. J. Schmidt, F. N. Büchi, *J. Electrochem. Soc.* **2019**, *166*, F270.
[47] G. Schmidt, M. Suermann, B. Bensmann, R. Hanke-Rauschenbach, I. Neuweiler, *J. Electrochem. Soc.* **2020**, *167*, 114511.
[48] J. Polonský, R. Kodým, P. Vágner, M. Paidar, B. Bensmann, K. Bouzek, *J. Appl. Electrochem.* **2017**, *47*, 1137.
[49] J. Kim, A. Ohira, *Membranes* **2021**, *11*, 330.
[50] H R. Corti, *Curr. Opin. Electrochem.* **2022**, *36*, 101109.
[51] A. V. Nikiforov, I. M. Petrushina, E. Christensen, N. V. Alexeev, A. V. Samokhin, N. J. Bjerrum, *Int. J. Hydrogen Energy* **2012**, *37*, 18591.
[52] L.-E. Owe, M. Tsypkin, S. Sunde, *Electrochim. Acta* **2011**, *58*, 231.
[53] J. O. Jensen, C. Chatzichristodoulou, E. Christensen, N. J. Bjerrum, Q. Li, in *Electrochemical Methods for Hydrogen Production* (Ed: K. Scott), The Royal Society of Chemistry, London, UK **2020**, Ch. 7.
[54] S. A. Grigoriev, P. Millet, S. A. Volobuev, V. N. Fateev, *Int. J. Hydrogen Energy* **2009**, *34*, 4968.
[55] H. Li, T. Fujigaya, H. Nakajima, A. Inada, K. Ito, *J. Power Sources* **2016**, *332*, 16.
[56] T. Schuler, T. J. Schmidt, F. N. Büchi, *J. Electrochem. Soc.* **2019**, *166*, F555.
[57] J. Seweryn, J. Biesdorf, T J. Schmidt, P. Boillat, *J. Electrochem. Soc.* **2016**, *163*, F3009.
[58] M A. Hoeh, T. Arlt, I. Manke, J. Banhart, D. L. Fritz, W. Maier, W. Lehnert, *Electrochem. commun.* **2015**, *55*, 55.
[59] G. Lu, S. L. Bernasek, J. Schwartz, *Surf. Sci.* **2000**, *458*, 80.
[60] J M. Spurgeon, N S. Lewis, *Energy Environ. Sci.* **2011**, *4*, 2993.
[61] T. Schuler, T. Kimura, T J. Schmidt, F N. Büchi, *Energy Environ. Sci.* **2020**, *13*, 2153.
[62] E. Borgardt, L. Giesenberg, M. Reska, M. Müller, K. Wippermann, M. Langemann, W. Lehnert, D. Stolten, *Int. J. Hydrogen Energy* **2019**, *44*, 23556.
[63] M. Stähler, A. Stähler, F. Scheepers, M. Carmo, W. Lehnert, D. Stolten, *Int. J. Hydrogen Energy* **2020**, *45*, 4008.
[64] Y. Cao, E. H. Bani Hani, I. B. Mansir, C. Diyoke, H A. Dhahad, *Int. J. Hydrogen Energy* **2021**, *47*, 26770.
[65] P. Ahmadi, I. Dincer, M. A. Rosen, *Int. J. Hydrogen Energy* **2013**, *38*, 1795.
[66] F. Musharavati, S. Khanmohammadi, I B. Mansir, *Int. J. Hydrogen Energy* **2021**, *47*, 25945.
[67] H. Nami, E. Akrami, *Energy Convers. Manag.* **2017**, *143*, 326.
[68] Y. E. Yuksel, M. Ozturk, I. Dincer, *Energy Convers. Manag.* **2016**, *119*, 109.
[69] B. Laoun, A. Khellaf, M W. Naceur, A M. Kannan, *Int. J. Hydrogen Energy* **2016**, *41*, 10120.
[70] F. Moradi Nafchi, E. Baniasadi, E. Afshari, N. Javani, *Int. J. Hydrogen Energy* **2018**, *43*, 5820.

[71] A. Badgett, M. Ruth, B. Pivovar in *Electrochemical Power Sources: Fundamentals, Systems, and Applications – Hydrogen Production by Water Electrolysis* (Eds: T. Smolinka, J. Garche), Elsevier, Amsterdam, Netherlands **2021**, Ch.10.
[72] *IRENA, Green Hydrogen Cost Reduction: Scaling up Electrolysers to Meet the 1.5°C Climate Goal*, IRENA, Masdar City, Abu Dhabi **2020**.
[73] S. Stiber, H. Balzer, A. Wierhake, F. J. Wirkert, J. Roth, U. Rost, M. Brodmann, J. K. Lee, A. Bazylak, W. Waiblinger, A. S. Gago, K. A. Friedrich, *Adv. Energy Mater.* **2021**, *11*, 2100630.
[74] H. Nguyen, C. Klose, L. Metzler, S. Vierrath, M. Breitwieser, *Adv. Energy Mater.* **2022**, *12*, 2103559.
[75] R. O'Hayre, S. Cha, W. G. Colella, F. B. Prinz, *Fuel Cell Fundamentals*, Wiley, New Jersey, USA **2016**.
[76] National Institute of Standards and Technology, https://webbook.nist.gov/chemistry/form-ser/ (accessed: December 2021).
[77] R. Hanke-Rauschenbach, B. Bensmann, P. Millet in *Compendium of Hydrogen Energy*, Vol. *1* (Eds: V. Subramani, A. Basile, T. Nejat Veziroğlu), Elsevier, Amsterdam, Netherlands **2015**, Ch. 7.
[78] U. Babic, *Doctoral Thesis*, ETH Zurich, USA, **2019**.
[79] C. Lamy, P. Millet, *J. Power Sources* **2020**, *447*, 227350.
[80] P. Millet in *Electrochemical Power Sources: Fundamentals, Systems, and Applications – Hydrogen Production by Water Electrolysis* (Eds: T. Smolinka, J. Garche), Elsevier, Amsterdam, Netherlands **2021**, Ch. 2.
[81] X. Sun, S. C. Simonsen, T. Norby, A. Chatzitakis, *Membranes* **2019**, *9*, 83.
[82] M. Carmo, D L. Fritz, J. Mergel, D. Stolten, *Int. J. Hydrogen Energy* **2013**, *38*, 4901.
[83] G. G. Gagliardi, A. Ibrahim, D. Borello, A. El-Kharouf, *Molecules* **2020**, *25*, 1712.
[84] C. Linkous, *Int. J. Hydrogen Energy* **1998**, *23*, 525.
[85] V. Antonucci, A. Di Blasi, V. Baglio, R. Ornelas, F. Matteucci, J. Ledesma-Garcia, L. G. Arriaga, A. S. Aricò, *Electrochim. Acta* **2008**, *53*, 7350.
[86] V. Baglio, R. Ornelas, F. Matteucci, F. Martina, G. Ciccarella, I. Zama, L. G. Arriaga, V. Antonucci, A. S. Aricò, *Fuel Cells* **2009**, *9*, 247.
[87] S. Siracusano, V. Baglio, M. A. Navarra, S. Panero, V. Antonucci, A. S. Aricò, *Int. J. Electrochem. Sci.* **2012**, *7*, 1532.
[88] H. Li, A. Inada, T. Fujigaya, H. Nakajima, K. Sasaki, K. Ito, *J. Power Sources* **2016**, *318*, 192.
[89] S. Choe, B.-S. Lee, M. K. Cho, H.-J. Kim, D. Henkensmeier, S. J. Yoo, J. Y. Kim, S. Y Lee, H. S. Park, J. H. Jang, *Appl. Catal., B* **2018**, *226*, 289.
[90] H. Ito, T. Maeda, A. Nakano, H. Takenaka, *Int. J. Hydrogen Energy* **2011**, *36*, 10527.
[91] J. T. Hinatsu, M. Mizuhata, H. Takenaka, *J. Electrochem. Soc.* **1994**, *141*, 1493.
[92] J. Mališ, P. Mazúr, M. Paidar, T. Bystron, K. Bouzek, *Int. J. Hydrogen Energy* **2016**, *41*, 2177.
[93] G. Gebel, P. Aldebert, M. Pineri, *Polymer* **1993**, *34*, 333.
[94] T. Sakai, H. Takenaka, N. Wakabayashi, Y. Kawami, E. Torikai, *J. Electrochem. Soc.* **1985**, *132*, 1328.
[95] N. Briguglio, F. Pantò, S. Siracusano, A. S. Aricò, *Electrochim. Acta* **2020**, *344*, 136153.
[96] N. H. Jalani, R. Datta, *J. Memb. Sci.* **2005**, *264*, 167.
[97] P. Shirvanian, F. Vvan Berkel, *Electrochem. Commun.* **2020**, *114*, 106704.
[98] A. Skulimowska, M. Dupont, M. Zaton, S. Sunde, L. Merlo, D. J. Jones, J. Rozière, *Int. J. Hydrogen Energy* **2014**, *39*, 6307.
[99] M. Cappadonia, J. W. Erning, S. M. S. Niaki, U. Stimming, *Solid State Ion.* **1995**, *77*, 65.
[100] J. Kim, A. Ohira, *Membranes* **2021**, *11*, 861.
[101] D. Aili, M. K. Hansen, C. Pan, Q. Li, E. Christensen, J. O. Jensen, N J. Bjerrum, *Int. J. Hydrogen Energy* **2011**, *36*, 6985.
[102] M. K. Hansen, D. Aili, E. Christensen, C. Pan, S. Eriksen, J. O. Jensen, J H. Von Barner, Q. Li, N J. Bjerrum, *Int. J. Hydrogen Energy* **2012**, *37*, 10992.
[103] J. Xu, Q. Li, M. K. Hansen, E. Christensen, A. L. Tomás García, G. Liu, X. Wang, N J. Bjerrum, *Int. J. Hydrogen Energy* **2012**, *37*, 18629.
[104] J. Xu, D. Aili, Q. Li, E. Christensen, J. O. Jensen, W. Zhang, M. K. Hansen, G. Liu, X. Wang, N J. Bjerrum, *Energy Environ. Sci.* **2014**, *7*, 820.
[105] D. Aili, R F. Savinell, J. O. Jensen, L N. Cleemann, N J. Bjerrum, Q. Li, *ChemElectroChem* **2014**, *1*, 1471.
[106] A. V. Nikiforov, I. M. Petrushina, E. Christensen, A. L. Tomás-García, N. J. Bjerrum, *Int. J. Hydrogen Energy* **2011**, *36*, 111.
[107] T M. Thampan, N. H. Jalani, P. Choi, R. Datta, *J. Electrochem. Soc.* **2005**, *152*, A316.
[108] X. Ge, F. Zhang, L. Wu, Z. Yang, T. Xu, *Macromolecules* **2022**, *55*, 3773.
[109] S. Siracusano, V. Baglio, I. Nicotera, L. Mazzapioda, A. S. Aricò, S. Panero, M. A. Navarra, *Int. J. Hydrogen Energy* **2017**, *42*, 27851.
[110] R. Scipioni, D. Gazzoli, F. Teocoli, O. Palumbo, A. Paolone, N. Ibris, S. Brutti, M. A. Navarra, *Membranes* **2014**, *4*, 123.
[111] M. K. Hansen, *PhD Thesis*, DTU, Denmark **2012**.
[112] L. Ghassemzadeh, G. Pace, V. Di Noto, K. Müller, *Phys Chem Chem Phys* **2011**, *13*, 9327.
[113] W. Xu, K. Scott, S. Basu, *J. Power Sources* **2011**, *196*, 8918.
[114] S. Subianto, M. Pica, M. Casciola, P. Cojocaru, L. Merlo, G. Hards, D. J. Jones, *J. Power Sources* **2013**, *233*, 216.
[115] S. Giancola, M. Zaton, Á. Reyes-Carmona, M. Dupont, A. Donnadio, S. Cavaliere, J. Rozière, D J. Jones, *J. Memb. Sci.* **2019**, *570*, 69.
[116] R. Savinell, E. Yeager, D. Tryk, U. Landau, J. Wainright, D. Weng, K. Lux, M. Litt, C. Rogers, *J. Electrochem. Soc.* **1994**, *141*, L46.
[117] C. Wieser, *Fuel Cells* **2004**, *4*, 245.
[118] M. Casciola, G. Alberti, M. Sganappa, R. Narducci, *J. Power Sources* **2016**, *162*, 141.
[119] I. Radev, G. Georgiev, V. Sinigersky, E. Slavcheva, *Int. J. Hydrogen Energy* **2008**, *33*, 4849.
[120] R. He, Q. Li, G. Xiao, N. J. Bjerrum, *J. Memb. Sci.* **2003**, *226*, 169.
[121] B. R. Matos, C. A. Goulart, E. I. Santiago, R. Muccillo, *Appl. Phys. Lett.* **2014**, *104*, 91904.
[122] K. D. Kreuer, M. Schuster, B. Obliers, O. Diat, U. Traub, A. Fuchs, U. Klock, S. J. Paddison, J. Maier, *J. Power Sources* **2008**, *178*, 499.
[123] P. Heimerdinger, A. Rosin, M. A. Danzer, T. Gerdes, *Membranes* **2019**, *9*, 62
[124] S. Shi, A Z. Weber, A. Kusoglu, *J. Memb. Sci.* **2016**, *516*, 123.
[125] R. W. Kopitzke, C. A. Linkous, H. R Anderson, G L. Nelson, *J. Electrochem. Soc.* **2000**, *147*, 1677.
[126] T A. Zawodzinski, M. Neeman, L O. Sillerud, S. Gottesfeld, *J. Phys. Chem.* **1991**, *95*, 6040.
[127] P. Mazúr, J. Polonský, M. Paidar, K. Bouzek, *Int. J. Hydrogen Energy* **2012**, *37*, 12081.
[128] L.-E. Owe, *Doctoral Thesis*, Norwegian University of Science and Technology, USA, **2011**.
[129] A. L. Tomás-García, Q. Li, J. O. Jensen, N. J. Bjerrum, *Int. J. Electrochem. Sci.* **2014**, *9*, 1016.
[130] A. L. Tomás-García, J. O. Jensen, N J. Bjerrum, Q. Li, *Electrochim. Acta* **2014**, *137*, 639.
[131] S. Kiemel, T. Smolinka, F. Lehner, J. Full, A. Sauer, R. Miehe, *Int. J. Energy Res.* **2021**, *45*, 9914.
[132] J. Polonský, P. Mazúr, M. Paidar, E. Christensen, K. Bouzek, *Int. J. Hydrogen Energy* **2014**, *39*, 3072.
[133] A. V. Nikiforov, A. L. Tomás García, I. M. Petrushina, E. Christensen, N. J. Bjerrum, *Int. J. Hydrogen Energy* **2011**, *36*, 5797.

[134] A. V. Nikiforov, I M. Petrushina, C B. Prag, J. Polonský, E. Christensen, N J. Bjerrum, *ECS Trans.* **2013**, *45*, 59.
[135] S. Geiger, O. Kasian, A. M. Mingers, K. J. J. Mayrhofer, S. Cherevko, *Sci. Rep.* **2017**, *7*, 4595.
[136] A. Hartig-Weiss, M. Miller, H. Beyer, A. Schmitt, A. Siebel, A. T. S. Freiberg, H. A. Gasteiger, H. A. El-Sayed, *ACS Appl. Nano Mater.* **2020**, *3*, 2185.
[137] M. Bernt, H. A. Gasteiger, *J. Electrochem. Soc.* **2016**, *163*, F3179.
[138] P. Trinke, B. Bensmann, R. Hanke-Rauschenbach, *Int. J. Hydrogen Energy* **2017**,*42*,14355.
[139] R. Omrani, B. Shabani, *Electrochim. Acta* **2021**, *377*, 138085.
[140] P. Trinke, G. P. Keeley, M. Carmo, B. Bensmann, R. Hanke-Rauschenbach, *J. Electrochem. Soc.* **2019**, *166*, F465.
[141] P. Trinke, B. Bensmann, S. Reichstein, R. Hanke-Rauschenbach, K. Sundmacher, *ECS Trans.* **2016**, *75*, 1081.
[142] S. A. Grigoriev, P. Millet, S. V. Korobtsev, V. I. Porembskiy, M. Pepic, C. Etievant, C. Puyenchet, V. N. Fateev, *Int. J. Hydrogen Energy* **2009**, *34*, 5986.
[143] S. Garbe, U. Babic, E. Nilsson, T. J. Schmidt, L. Gubler, *J. Electrochem. Soc.* **2019**, *166*, F873.
[144] D. Stolten, D. Emonts, *Hydrogen Science and Engineering*, (Ed.: D. Stolten, B. Emonts), Wiley-VCH Verlag GmbH & Co. KGaA, Markono Print Media Pte Ltd, Singapore **2016**.
[145] M. S. Thomassen, A. H. Reksten, A. O. Barnett, T. Khozy, K. Ayers in *Electrochemical Power Sources: Fundamentals, Systems, and Applications – Hydrogen Production by Water Electrolysis* (Eds: T. Smolinka, J. Garche), Elsevier, Amsterdam, Netherlands **2021**, Ch.6.
[146] C. Rakousky, U. Reimer, K. Wippermann, M. Carmo, W. Lueke, D. Stolten, *J. Power Sources* **2016**, *326*, 120.
[147] C. Liu, K. Wippermann, M. Rasinski, Y. Suo, M. Shviro, M. Carmo, W. Lehnert, *ACS Appl. Mater. Interfaces* **2021**, *13*, 16182.
[148] A. H. Jensen, E. Christensen, J. H. Von Barner, *ECS Electrochem. Lett.* **2014**, *3*, F50.
[149] H. Li, H. Nakajima, A. Inada, K. Ito, *Int. J. Hydrogen Energy* **2018**, *43*, 8600.
[150] H. Ito, T. Maeda, A. Nakano, Y. Hasegawa, N. Yokoi, C. M. Hwang, M. Ishida, A. Kato, T. Yoshida, *Int. J. Hydrogen Energy* **2010**, *35*, 9550.
[151] H. Li, A. Inada, H. Nakajima, K. Ito, *ECS Trans.* **2015**, *69*, 3.
[152] O. F. Selamet, U. Pasaogullari, D. Spernjak, D. S. Hussey, D. L. Jacobson, M. D. Mat, *Int. J. Hydrogen Energy* **2013**, *38*, 5823.
[153] C. Lee, R. Banerjee, N. Ge, J. K. Lee, B. Zhao, E. Baltic, J M. LaManna, D. S. Hussey, D. L. Jacobson, R. Abouatallah, R. Wang, A. Bazylak, *Electrochim. Acta* **2018**, *279*, 91.
[154] H. Ito, T. Maeda, A. Nakano, C. M. Hwang, M. Ishida, A. Kato, T. Yoshida, *Int. J. Hydrogen* **2012**, *37*, 7418.
[155] Na Li, S. S. Araya, S. K. Kær, *Int. J. Hydrogen Energy* **2019**, *44*, 12952.
[156] S. Lædre, O. E. Kongstein, A. Oedegaard, H. Karoliussen, F. Seland, *Int. J. Hydrogen Energy* **2017**, *42*, 2713.
[157] A. Rohatgi, WebPlotDigitizer, https://automeris.io/WebPlotDigitizer (accessed: December 2020).
[158] D. Aili, H. Becker, U. Reimer, J. W. Andreasen, L. N. Cleemann, J. O. Jensen, C. Pan, X. Wang, W. Lehnert, Q. Li, *J. Electrochem. Soc.* **2020**, *167*, 134507.
[159] D. Zhao, Q. He, J. Yu, M. Guo, J. Fu, Xi Li, M. Ni, *Int. J. Hydrogen Energy* **2022**, *47*, 8687.
[160] D. Zhao, Q. He, X. Wu, Y. Xu, J. Jiang, X. Li, M. Li, *Int. J. Green Energy* **2022**, *19*, 919.
[161] J. Kai, R. Saito, K. Terabaru, H. Li, H. Nakajima, K. Ito, *J. Electrochem. Soc.* **2019**, *166*, F246.
[162] S. Toghyani, E. Afshari, E. Baniasadi, S. A. Atyabi, G. F. Naterer, *Energy* **2018**, *152*, 237.
[163] S. Toghyani, E. Baniasadi, E. Afshari, *Int. J. Hydrogen Energy* **2019**, *44*, 31731.
[164] S. Toghyani, E. Baniasadi, E. Afshari, N. Javani, *Int. J. Hydrogen Energy* **2020**, *60*, 34993.
[165] D. de Haro Ruiz, A. P. Sasmito, T. Shamim, *ECS Trans.* **2013**, *58*, 99.
[166] D. Zhao, Q. He, J. Yu, J. Jiang, X. Li, M. Ni, *Int. J. Hydrogen Energy* **2020**, *45*, 26613.
[167] D. Zhao, Z. Xia, M. Guo, Q. He, Q. Xu, X. Li, M. Ni, *Int. J. Hydrogen Energy* **2022**, *47*, 22302.
[168] K. E. Ayers, E. B. Anderson, C. B. Capuano, B. D. Carter, L. T. Dalton, G. Hanlon, J. Manco, M. Niedzwiekci, *ECS Trans.* **2010**, *33*, 3.
[169] S. Garbe, J. Futter, A. Agarwal, M. Tarik, A. A. Mularczyk, T. J. Schmidt, L. Gubler, *J. Electrochem. Soc.* **2021**, *168*, 044515.
[170] S. H. Frensch, F. Fouda-Onana, G. Serre, D. Thoby, S. S. Araya, S. K. Kær, *Int. J. Hydrogen Energy* **2019**, *44*, 29889.
[171] A. Laconti, H. Liu, C. Mittelsteadt, R. Mcdonald, *ECS Trans.* **2006**, *1*, 199.
[172] S. H. Frensch, G. Serre, F. Fouda-Onana, H. C. Jensen, M. L. Christensen, S. S. Araya, S. K. Kær, *J. Power Sources* **2019**, *420*, 54.
[173] F. Fouda-Onana, M. Chandesris, V. Médeau, S. Chelghoum, D. Thoby, N. Guillet, *Int. J. Hydrogen Energy* **2016**, *41*, 16627.
[174] M. Chandesris, V. Médeau, N. Guillet, S. Chelghoum, D. Thoby, F. Fouda-Onana, *Int. J. Hydrogen Energy* **2015**, *40*, 1353.
[175] P. Marocco, K. Sundseth, T. Aarhaug, A. Lanzini, M. Santarelli, A. O. Barnett, M. Thomassen, *J. Power Sources* **2021**, *483*, 229179.
[176] J.-T. Wang, W.-W. Wang, C. Wang, Z.-Q. Mao, *Int. J. Hydrogen Energy* **2012**, *37*, 12069.
[177] C. Liu, M. Carmo, G. Bender, A. Everwand, T. Lickert, J. L. Young, T. Smolinka, D. Stolten, W. Lehnert, *Electrochem Commun.* **2018**, *97*, 96.

David Aili has an educational background in chemistry, and obtained his PhD from DTU Chemistry in 2011. Following a period in the polymer industry in Sweden, he joined DTU Energy in 2012. His field of research spans from fundamental chemistry and polymer science to catalysis and electrochemical conversion in the context of electrolysis, power-to-X, CO_2 capture/utilization, fuel cells, and flow batteries.